Real-time Detection of Dopamine – Aptamer Interactions in a Nanopore: A Label-free Toolkit for Study of Nucleic-acid-based Molecular Sensors.

A Dissertation

presented to

the Faculty of the Graduate School

at the University of Missouri-Columbia

In Partial Fulfillment

of the Requirements for the Degree

Doctor of Philosophy

---

by

GEORGE RUGARE CHINGARANDE

Dr Kevin Gillis, Dissertation Supervisor

Dr Liqun Gu, Dissertation co-supervisor

JULY 2021

The undersigned, appointed by the dean of the Graduate School, have examined the dissertation entitled

REAL-TIME DETECTION OF DOPAMINE – APTAMER INTERACTIONS IN A

NANOPORE: A LABEL-FREE TOOLKIT FOR STUDY OF NUCLEIC-ACID-BASED MOLECULAR SENSORS.

presented by George Rugare Chingarande,

a candidate for the degree of Doctor of Philosophy

and hereby certify that, in their opinion, it is worthy of acceptance.

_____

Professor Kevin Gillis

_____

Professor Liqun Gu

_____

Professor IIker Ozden

_____

Professor Shingua Ding

_____

Professor Shi-jie Chen

DEDICATION

I would like to acknowledge and at the same time dedicate this work to the following people:

My parents Godfrey T and Julia W Chingarande. Without them I wouldn't have been born. They taught me the value of being a talent-plus person by exhorting me to add to my talents the 5Cs. Christ, who strengthens me and through whom I can do all things. Character, without which every achievement stinks. Courage-the immutable truth that by courageously challenging oneself to take acts of boldness everyday one can alter the circumstances of his life. Continuous improvement-the habit of never going to bed without asking oneself how have I become better and more today. And Conscious endeavor-the most encouraging fact of all that there is no end to human potential and man can elevate his station in life by conscious endeavor. It is these 5Cs that continue to guide me and inspired me to pursue this PhD. They continue to inspire me that I can now become a Talent-plus and a PhD-PLUS person by adding these 5Cs to the PhD.

My wife, Anna, for not only being my dearest, ever-present partner in pursuit of self-actualization, but also supporting me and putting up with my innumerable idiosyncrasies and insufferable foibles.

My son, Prince Tinashe and daughter Blessings Tatenda-from whom I learn much every day and whose smiles and wits make me feel like moving mountains.

All my teachers, who are too numerous to mention, but each contributed in a very significant way to who I am today.

To the IIE and Fulbright program, without whose financial support, the burden of financing graduate studies would have been insuperable.

ACKNOWLEDGMENTS

This PhD adventure was one convoluted odyssey. I owe a debt of gratitude to Dr Jinglu Tan for recommending Dr Kevin Gillis to me and introducing me to Dr Gillis. It was the most consequential event of my graduate school years.

I would like to thank Dr Kevin Gillis for being a generous and patient mentor. Above all, I will always remember with fondness his knack for making the complex simple and his incisive analyses that not only illuminate but also inspire one to want to know more. Before I met him, I was told that his reputation for scientific rigor and integrity precedes him. He did not disappoint.

Special mention goes to Dr Liqun Gu who served as my co-advisor. His passion for science was infectious and his relentless pursuit of new ideas was amazing. His contribution in terms of insights and ideas was immeasurable.

Xin Alice Liu took time to teach me the basics and all the little tricks of the trade. For that I am most grateful

Finally, I would like to thank my other committee members Dr IIker Ozden, Dr Shi-jie Chen and Dr Shingua Ding. Their insights, inputs and dedication are greatly appreciated.

Table of Contents

List of Figures

ABSTRACT

Understanding how small molecules regulate nucleic acid structures is important in both bio-mechanism elucidation and biotechnological applications. Through the conformational variation, native nucleic acid motifs can be used as the targets to screen therapeutic compounds; In vitro selected aptamers can be used to detect small molecule biomarkers such as neurotransmitters and hormones, and ligand-triggered riboswitches can be designed to control gene expressions. All these applications need a rapid universal platform to detect nucleic acid conformational change in response to small molecule binding. Here we propose a label-free, non-invasive, and modular aptamer-inlaid nanopore capable of revealing time-resolved single nucleic acid molecule conformational transitions at the millisecond resolution. When a dopamine aptamer is docked in the MspA protein pore, the ion current through the pore can characteristically vary as the aptamer transitions between different conformations, recording a sequence of current fingerprints for binding and release of single neurotransmitter molecules from the aptamer. Without the need to mix the aptamer and the ligand, the sensor can quantify the target neurotransmitter, discriminate between different neurotransmitters, assay nucleic acid-ligand interactions, elucidate the ligand selectivity mechanism and pinpoint the ligand docking motifs in the aptamer, offering a potential nanopore toolbox for multiple small molecule biomarkers detection and screening nucleic acid-targeted small molecule regulators. Finally, we optimize the sensitivity of the nanopore sensor by employing divalent ions.

Chapter One

Introduction

1.1. Nanopore Sensing

The first two decades of the new millennium ushered in a thrust towards personalized and precision medicine. It is estimated that the total worldwide market share for personalized medicine will exceed 3.18 trillion dollars by 2025(Davis et al., 2009)[1]. At its core, personalized medicine involves the customization of medical care to the individual, while precision medicine is crafted to optimize efficiency and therapeutic benefit for individuals and sometimes particular groups of patients. Both personalized medicine and precision medicine rely, to a large extent, on the understanding of and elucidation of the molecular basis of disease. The development of tools to aid this understanding and to catalyze development of therapeutics is of paramount importance. Nanopore sensing is one such tool and holds great promise.

Nanopore sensing has evolved into a useful single-molecule tool to investigate the features of biomolecules at the molecular level. It is predicated on the measurement of changes in ionic current as charged biomolecules immersed in an electrolyte translocate through a pore that is comparable in size to the translocating molecule. Fig.1 shows a cartoon representation of a protein nanopore system which consists of a chamber divided into two compartments (*cis&trans*) by a Teflon membrane with a small aperture that is spanned by a lipid bilayer membrane. The chambers are filled with an electrolyte solution of cations and a potential is applied between the compartments with the *cis* being the reference or the ground. When a potential difference is applied protein pores added to the *cis* side insert in the membrane thereby creating a pathway between the compartments. Biomolecules placed on the cis side move from the bulk solution to the entrance of the pore, where they must overcome a free energy barrier so as to thread into the

nanometre-sized pore. The presence of a biomolecule in the pore causes a partial or complete blockade which manifests as a short-lived current modulation. Analysis of the blockage current, duration of blockage, frequencies, and amplitudes of the blockade events yields information on the properties of the target molecule in real time. Information such as size, conformation, structure, charge, geometry, and interactions with other molecules can often be inferred.

Different biomolecules block the current to different levels and for different durations, thus making it possible to discriminate between them. The biomolecule is trapped in the pore for a dwell time t_D. The time between two successive events is shown as Δt in Fig 1a. If t_D is small (fast translocation time), it's difficult to resolve the event due to limitations in amplifier bandwidth and signal-to-noise ratio. If Δt is too large, fewer events are captured. Different concentrations of different ions produce differential current blockage. ***Currently a key limitation of nanopore sensing is the superfast translocation rate of nucleic acids (1–7ms/ base).***

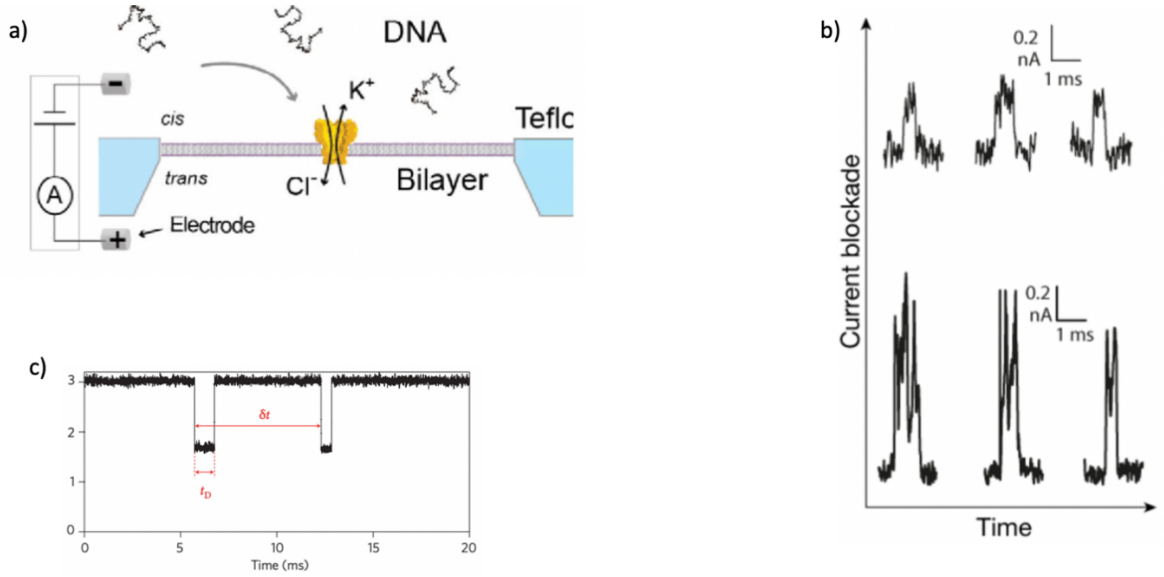

Fig 1. 1: Nanopore system cartoon representation.

a) The experimental set up. The bilayer is established across a ~20μm Teflon aperture. b) Representative traces c) The time between successive events δt and dwell time t_D diagrammatically illustrated.

molecules. Nanopore sensing has been applied for the detection of various biomolecules, including oligonucleotides, peptides, oligosaccharides, organic molecules, and disease-related proteins[4].

Nanopore sensing is impacting the practice of medicine in at least three areas namely, biomolecular detection, drug development and synthetic biology. In aptamer-based biomolecular detection, aptamers are placed on the cis side of the chamber and the molecule under investigation is placed on the trans side. Target molecules include small molecules, neurotransmitters, metabolites, hormones, and drugs. Protein nanopore biosensing has a myriad of advantages. The aptamer and the ligand are placed in opposite chambers of the nano-sensor. Consequently, they do not interact in the bulk solution, but only when translocating the nanopore. One aptamer molecule can be used to detect many ligand molecules through sequential binding and unbinding reactions. Additionally, since aptamers bind with high affinity and specificity to target molecules, it is possible to identify and quantify the ligand. Moreover, detection is fast because there is no need to wait for equilibrium. Additionally, both aptamer and ligand can be freely changed thus facilitating high throughput screening, which facilitates pharmaceutical drug discovery.

Nanopore sensing provides insightful paths to disease diagnosis and rational drug development. In recent years, isolation and interrogation of ribonucleic acid (RNA) molecules has revolutionized biology[5]. For instance, low abundance RNA molecules (e.g., microRNA, long noncoding RNA) have been shown to exhibit diverse functional roles in cell maintenance[6]. RNA function, just like proteins, is associated with the formation of elaborate three-dimensional

structures. Conformational changes contain useful information for medicinal purposes and drug development. Nanopore sensing is a useful tool in investigating conformational changes and by extension drug development. For example, the hepatitis C virus (HCV) causes hepatitis C in humans, a life-threatening liver inflammation that occurs in roughly 80% of patients infected with HCV[7]. There is currently no vaccine for HCV, and before the approval of direct antiviral drugs, leading treatments were only curative in 50% of patients[8]. HCV replicates by binding to host cell ribosomes using an internal ribosome entry site (IRES) RNA motif[9]. The IRES domain is a highly conserved motif that allows efficient, independent translation initiation at the ribosome by virtue of its elbow structure. This information has been used to develop drugs that inhibit IRES activity[9].

Generally, bacterial riboswitch RNAs are attractive targets for novel antibiotics against antibiotic-resistant super-bacteria. Their binding to cognate metabolites is essential for the regulation of bacterial gene expression. Despite the importance of RNAs as therapeutic targets, the development of RNA-targeted, small molecule drugs is limited by current biophysical methods. Nanopore sensing offers a more pristine and valuable platform for ultrasensitive, label-free, and single-molecule-based drug screening against therapeutic RNA targets.

At the core of synthetic biology is the idea of engineering biological systems for a desired outcome. It has assumed increased importance in a variety of applications, including but not limited to the production of therapeutics[10], fine chemicals[11,12], biofuels[13,14] and biomaterials[15,16] or the generation of novel functional organisms like biosensors[17]or computers [18]. The process typically involves construction of synthesized DNA into specifically designed constructs, which are often large and complex. The availability of inexpensive DNA synthesis and assembly

methods coupled to high-throughput automation approaches allows expeditious synthesis of any designed sequence.

There are a wide variety of DNA assembly techniques available to create synthetic DNA constructs, including Ligase Cycling Reaction (LCR), Golden Gate, BioBricks, Gibson assembly (and other similar methods based on joining homologous ends) and recombination [18,19]. Advances in design and synthesis have created a demand for high throughput methods for verifying correctly assembled constructs. This need can be addressed, to some extent by using Next-generation sequencing. However Next Generation Sequencing requires expensive hardware and convoluted data analysis. Consequently, in house use of this technology is limited. A cost-effective alternative offering high throughput capability is necessary. Nanopore sensing is one such approach.

1.2 Lipid Membranes and the MspA nanopore.

The cell is considered the fundamental unit of living organisms. All cells contain a membrane that separates the environment inside the cell from the external environment. To function properly, cells need to import metabolites and energy sources and expel wastes and toxic substances. This transfer of substances is facilitated by membrane proteins such as ion channels, pumps, and transporters.

Two components of the cell membranes are important for the purposes of this work. These are the lipid bilayer and species-specific integral membrane proteins. As the name suggests the bilayer is made up of two layers of lipid. Each lipid molecule contains a *hydrophilic* head and a *hydrophobic* tail. The repulsion of the tails by water abetted by a slight

attraction between them causes them to aggregate together. This creates a configuration in which the heads face the fluid and the tails face each other thereby creating a barrier between two fluid compartments such as the inside and outside of the cell. The lipid used in this work is 1,2-diphytanoyl-sn-glycero-3-phosphocholine. Broadly there are two types of membrane proteins that act as pores. The first group of proteins which span both leaflets of the bilayer membrane facilitate the controlled passage of ions from one side of the membrane to the other. These proteins are known as "ion channels." The second group which typically have nanometer sized openings allow for the uncontrolled passage of anything small enough to fit through them and are known as "porins." Mycobacterium smegmatis porin A (MspA) is one of these.

MspA is a water filled octameric protein[21]. The three-dimensional structure of the MspA protein is shown in Fig 1.2. The function of the pore is to allow passage of hydrophilic molecules of appropriate size and charge into and out of the cell[22]. The constriction of the pore is 1.2nm wide. This is wide enough to allow ssDNA translocation but too narrow for dsDNA translocation. This characteristic has been exploited in DNA sequencing.

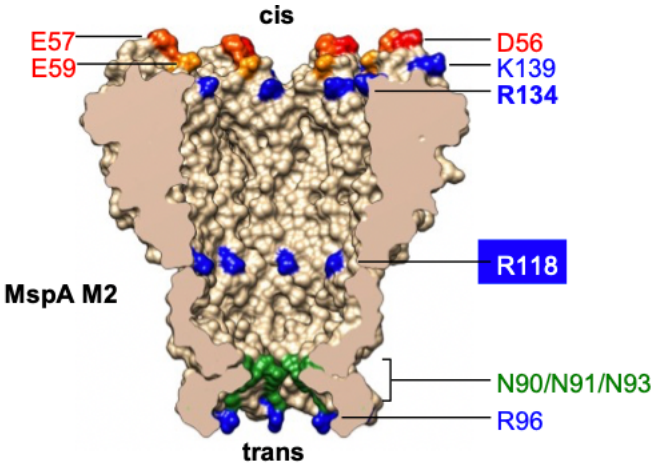

Fig 1. 2: The MspA pore structure.

Butler et. al. (2008)[23] demonstrated that the MspA wild type could be employed as a DNA sequencing tool. It was noted that the wild-type pore would spontaneously gate at applied bias voltages above 60 mV. Additionally, no ssDNA was detectable. They hypothesized that given that the DNA has a negative phosphate backbone, electrostatic interactions between the negative charges lining the constriction were preventing ssDNA from entering and translocating through the pore. Mutations were made at positions D90N/D91N/D93N (see Fig 1.2), changing the negatively charged aspartic acid residues lining the constriction to neutral asparagine residues. This eliminated spontaneous voltage gating and allowed ssDNA to translocate through the pore. Further mutations at positions E139K/D134R/D188R, added positively charged amino acids in the vestibule and around the top of MspA. This alteration produced M2-MspA pore which effectively enhanced the capture rate of DNA at lower voltage biases. The current work was based on M2-MspA. The internal charge distributions of the M2-MspA are shown in Fig 1.2. The negative charges are red and positive charges are blue. Green is neutral.

1.3 Neurotransmitters

Neurotransmitters are small molecules that relay chemical messages between neurons cells. Neurochemical signaling is central to the functioning of the brain and central nervous system and is critical for the diagnosis and treatment of neuronal disorders. Signaling at synapses via transmitter release can occur within a millisecond. Briefly, the transmitter is synthesized *via* a presynaptic process and packaged at high concentrations within vesicles in the presynaptic terminal. This is followed by release of neurotransmitter from the presynaptic cell into the synaptic cleft by Ca^{2+} triggered exocytosis. After release, the transmitter binds to receptors on the postsynaptic cell or to auto-receptors on the presynaptic cell. Neurotransmitter binding to receptors leads to either opening of ion channels (ionotropic responses) or generation of second-messenger signals (metabotropic responses). Responses to transmitter release are often brief due

to either diffusion of the transmitter, degradation by enzymes in the synaptic cleft, or uptake into cells by specific transporters.

1.3.1 Dopamine Synthesis and Storage

Dopamine (DA) is an important neurotransmitter in the mammalian central nervous system (CNS). Its criticality is underlined by its implication in a plethora of neurobehavioral disorders. In Parkinson's disease, typical clinical symptoms such as resting tremor, rigidity, bradykinesia (a gradual slowness of spontaneous movement), and loss of postural reflexes (poor balance and motor coordination) are linked to depletion of dopamine in the corpus striatum[24]. In Huntington's disease the dopamine effect is biphasic. In the early stage an increase in dopamine levels leads to hyperkinetic disorders such as chorea. However, in the later stage dopamine deficits results in hypokinesia[25]. In schizophrenia dopamine abnormalities have been reported in the mesolimbic and prefrontal brain region[26]. Evidence exists to support the role of dopamine in the etiology of post-traumatic stress disorder[27], depression[28], substance abuse[29], and eating disorders[30].

Dopamine is biosynthesized in dopaminergic neuron terminals. In the reward pathway, the production of dopamine takes place in the cell bodies in the ventral tegmental area, from where it is released into the nucleus accumbens and prefrontal cortex. The in vivo concentration of dopamine in the ventral tegmental area is 4.8 ± 1.5 nM, while in red nucleus, it is 0.5 ± 1.5 nM[31]. The pathway for motor functions is different. In this pathway, the substantia nigra cell bodies are responsible for the production and discharge of DA into the striatum. Dopamine is, therefore, considered as an important biomarker for studies of behavior and diseases, their diagnosis, therapy and prognosis. Like all biomarkers, assays must be developed for the measurement of dopamine at its physiological relevant levels (in human serum/blood plasma ranging between a basal level of 1.3 nM and 0.9−6 μM as found in L-DOPA-treated Parkinson's

patients;[32] and in the brain ranging between a basal 10 nM level and 1 μM as reached during dopamine release).[33]

1.3.2 Sensors and Biosensors for dopamine detection.

The low concentrations in physiological conditions complicate the measurement of dopamine. The problem is further compounded by the existence of interferents such as uracil and uric acid. At pH 7.0 (pK_a 8.9) dopamine is positively charged[33].

Several methods have been developed for the measurement of dopamine. These include, ultrahigh performance liquid chromatography mass spectroscopy, electrochemistry, positron emission tomography scanning, fluorescent enzyme-based biosensors, micro-dialysis, and Field-effect (FET) transistors. Each of these methods has inherent drawbacks. Although mass spectroscopy instrumentation is widely available, for most researchers, it remains difficult for in situ monitoring of dopamine with a high specificity and high temporal and spatial resolution, which are critical for the detection of dopamine[33]. Micro-dialysis suffers from poor temporal resolution. Electrochemical approaches are hampered by the fact that it is not easy to distinguish dopamine from analogues such as norepinephrine, epinephrine, L-Dopa, D-tyrosine, L-tyrosine, and tyramine. These neurotransmitters share the same catechol group as dopamine and have electrochemical signatures like dopamine. The problem is further compounded by the existence of interferents such as uracil and uric acid. Positron emission tomography scanning requires the injection of trace amounts of radioactive substances into the subject. Subjects are often wary of exposure to radiation. FET-based biosensors have desirable characteristics, such as rapid label-free electrical detection, low power consumption, portability, inexpensive mass production, and the possibility of on-chip integration of both sensor and measurement systems but suffer from poor stability and selectivity[34]. Enzymatic based sensors are associated with high cost,

complicated production procedures, and short shelf lives[31]. Aptamer based sensors do not suffer from these drawbacks.

1.3.3 Aptamer based biosensors.

Aptamers are single-stranded nucleic acids that can bind target molecules with high affinity and specificity[35]. Aptamer binding invariably yields a conformational change, which can be exploited for developing specific biosensors with a fast response[36-39]. Additionally, nucleic acids have programmable and predictable secondary structures. This trait can be exploited to make versatile biosensor designs. Aptamers are particularly adept at small molecules binding[40,41]. Small molecule metabolites are known to bind to naturally occurring aptamers in riboswitches[46].

Mannironi et al[42] isolated the first dopamine aptamer by exposing dopamine, immobilized via its primary amine group on a column, to a large library containing random RNA sequences. Employing this RNA aptamer sequence, a DNA aptamer was produced [43]. It was found that the DNA aptamer bound dopamine tighter than the RNA aptamer[45]. Recently, a new aptamer was developed using the structure-switch mechanism which allows for easy sensor design (Fig 1.3)[44].

Fig 1. 3: The secondary structure of the dopamine aptamers obtained from direct selection:

The current work is based on the aptamer depicted in Fig 1.3.

1.4 Conclusion

Many strides have been made in the development of nanopore sensor technology. This chapter presented a brief overview on the various aspects of neurotransmitter detection using nanopore sensor approaches. The rest of the dissertation is arranged as follows:

Chapter 2 presents a synopsis of the materials and methods used.

Chapter 3 presents a nanopore based platform for the detection and measurement of neurotransmitters and probing the conformational states and kinetics.

Chapter 4 articulates attempts to enhance sensitivity of the nanopore sensor detection and measurement of dopamine.

Finally in chapter 5 future directions are presented.

References

1. Davis, J. C., Furstenthal, L., Desai, A. A., Norris, T., Sutaria, S., Fleming, E., & Ma, P. (2009). The microeconomics of personalized medicine: today's challenge and tomorrow's promise. *Nature reviews Drug discovery*, *8*(4), 279-286.

2. Derrington, I. M., Butler, T. Z., Collins, M. D., Manrao, E., Pavlenok, M., Niederweis, M., & Gundlach, J. H. (2010). Nanopore DNA sequencing with MspA. *Proceedings of the National Academy of Sciences*, *107*(37), 16060-16065.

3. Kowalczyk, S. W., Wells, D. B., Aksimentiev, A., & Dekker, C. (2012). Slowing down DNA translocation through a nanopore in lithium chloride. *Nano letters*, *12*(2), 1038-1044.

4. Venkatesan, B. M., & Bashir, R. (2011). Nanopore sensors for nucleic acid analysis. *Nature nanotechnology*, *6*(10), 615-624.

5. Cameron, D. E., Bashor, C. J., & Collins, J. J. (2014). A brief history of synthetic biology. *Nature Reviews Microbiology*, *12*(5), 381-390.

6. Grosjean, H. (2005). *Fine-tuning of RNA functions by modification and editing* (Vol. 24, p. 442). H. Grosjean (Ed.). Berlin: Springer.

7. Seeff, L. B., & Hoofnagle, J. H. (2003). The National Institutes of Health Consensus Development Conference: Management of Hepatitis C 2002. *Clinics in liver disease*, *7*(1), 261-287.

8. Hagan, L. M., Wolpe, P. R., & Schinazi, R. F. (2013). Treatment as prevention and cure towards global eradication of hepatitis C virus. *Trends in microbiology*, *21*(12), 625-633.

9. Tsukiyama-Kohara, K., Iizuka, N., Kohara, M., & Nomoto, A. (1992). Internal ribosome entry site within hepatitis C virus RNA. *Journal of virology*, *66*(3), 1476-1483.

10. Paddon, C. J., Westfall, P. J., Pitera, D. J., Benjamin, K., Fisher, K., McPhee, D., ... & Newman, J. D. (2013). High-level semi-synthetic production of the potent antimalarial artemisinin. *Nature*, *496*(7446), 528-532.

11. Nicholas, J. W. (2016). Bioinformatics for the synthetic biology of natural products: integrating across the Design–Build–Test cycle. *Natural product reports*, *33*(8), 925-932.

12. Carbonell,P., Jervis,A.J., Robinson,C.J., Yan,C., Dunstan,M., Swainston,N., Vinaixa,M., Hollywood,K.A., Currin,A., Rattray,N.J.W. et al. (2018) An automated Design-Build-Test-Learn pipeline for enhanced microbial production of fine chemicals. Commun. Biol., 1, 66.

13. Khara, B., Menon, N., Levy, C., Mansell, D., Das, D., Marsh, E. N. G., ... & Scrutton, N. S. (2013). Production of propane and other short-chain alkanes by structure-based engineering of ligand specificity in aldehyde-deformylating oxygenase. *ChemBioChem*, *14*(10), 1204.
14. Jang, Y. S., Park, J. M., Choi, S., Choi, Y. J., Cho, J. H., & Lee, S. Y. (2012). Engineering of microorganisms for the production of biofuels and perspectives based on systems metabolic engineering approaches. *Biotechnology advances*, *30*(5), 989-1000.
15. Ahmed,S.T., Leferink,N.G.H. and Scrutton,N.S. (2019) Chemo-enzymatic routes towards the synthesis of bio-based monomers and polymers. Mol. Catal., 467, 95–110.
16. Roberts, A. D., Finnigan, W., Wolde-Michael, E., Kelly, P., Blaker, J. J., Hay, S., ... & Scrutton, N. S. (2019). Synthetic biology for fibers, adhesives, and active camouflage materials in protection and aerospace. *MRS communications*, *9*(2), 486-504.
17. Trabelsi, H., Koch, M., & Faulon, J. L. (2018). Building a minimal and generalizable model of transcription factor–based biosensors: Showcasing flavonoids. *Biotechnology and bioengineering*, *115*(9), 2292-2304.
18. Currin, A., Korovin, K., Ababi, M., Roper, K., Kell, D. B., Day, P. J., & King, R. D. (2017). Computing exponentially faster: implementing a non-deterministic universal Turing machine using DNA. *Journal of the Royal Society Interface*, *14*(128), 20160990.
19. Ellis, T., Adie, T., & Baldwin, G. S. (2011). DNA assembly for synthetic biology: from parts to pathways and beyond. *Integrative Biology*, *3*(2), 109-118.
20. Yèagle, P. L. (1989). Lipid regulation of cell membrane structure and function. *The FASEB journal*, *3*(7), 1833-1842.
21. Faller, M., Niederweis, M., & Schulz, G. E. (2004). The structure of a mycobacterial outer-membrane channel. *Science*, *303*(5661), 1189-1192.
22. Stahl, C., Kubetzko, S., Kaps, I., Seeber, S., Engelhardt, H., & Niederweis, M. (2001). MspA provides the main hydrophilic pathway through the cell wall of Mycobacterium smegmatis. *Molecular microbiology*, *40*(2), 451-464.
23. Fleming, S. J. (2018). *Probing nanopore-DNA interactions with MspA* (Doctoral dissertation, Harvard University).
24. Gilman, S. (2011). *Neurobiology of disease*. Elsevier.

25. Reiner, A., Shelby, E., Wang, H., DeMarch, Z., Deng, Y., Guley, N. H., ... & Faull, R. L. (2013). Striatal parvalbuminergic neurons are lost in Huntington's disease: implications for dystonia. *Movement Disorders*, *28*(12), 1691-1699.
26. Perez-Costas, E., Melendez-Ferro, M., & Roberts, R. C. (2010). Basal ganglia pathology in schizophrenia: dopamine connections and anomalies. *Journal of neurochemistry*, *113*(2), 287-302.
27. Drury, S. S., Theall, K. P., Keats, B. J., & Scheeringa, M. (2009). The role of the dopamine transporter (DAT) in the development of PTSD in preschool children. *Journal of Traumatic Stress: Official Publication of the International Society for Traumatic Stress Studies*, *22*(6), 534-539.
28. Brown, A. S., & Gershon, S. (1993). Dopamine and depression. *Journal of Neural Transmission/General Section JNT*, *91*(2), 75-109.
29. Volkow, N. D., Fowler, J. S., Wang, G. J., Swanson, J. M., & Telang, F. (2007). Dopamine in drug abuse and addiction: results of imaging studies and treatment implications. *Archives of neurology*, *64*(11), 1575-1579.
30. Blum, K., Oscar-Berman, M., Barh, D., Giordano, J., & Gold, M. S. (2013). Dopamine genetics and function in food and substance abuse. *Journal of genetic syndrome & gene therapy*, *4*(121).
31. Slaney, T. R., Mabrouk, O. S., Porter-Stransky, K. A., Aragona, B. J., & Kennedy, R. T. (2013). Chemical gradients within brain extracellular space measured using low flow push–pull perfusion sampling in vivo. *ACS chemical neuroscience*, *4*(2), 321-329.
32. Kissinger, P. T., Hart, J. B., & Adams, R. N. (1973). Voltammetry in brain tissue—a new neurophysiological measurement. *Brain research*, *55*(1), 209-213.
33. Michael, A. C., & Borland, L. (Eds.). (2006). Electrochemical methods for neuroscience.
34. Sarkar, D., Liu, W., Xie, X., Anselmo, A. C., Mitragotri, S., & Banerjee, K. (2014). MoS2 field-effect transistor for next-generation label-free biosensors. *ACS nano*, *8*(4), 3992-4003.
35. Wilson, D. S., & Szostak, J. W. (1999). In vitro selection of functional nucleic acids. *Annual review of biochemistry*, *68*(1), 611-647.
36. Hermann, T., & Patel, D. J. (2000). Adaptive recognition by nucleic acid aptamers. *Science*, *287*(5454), 820-825.

37. Liu, J., Cao, Z., & Lu, Y. (2009). Functional nucleic acid sensors. *Chemical reviews*, *109*(5), 1948–1998.
38. Zhou, W., Huang, P. J. J., Ding, J., & Liu, J. (2014). Aptamer-based biosensors for biomedical diagnostics. *Analyst*, *139*(11), 2627-2640.
39. Pang, X., Cui, C., Wan, S., Jiang, Y., Zhang, L., Xia, L., ... & Tan, W. (2018). Bioapplications of cell-SELEX-generated aptamers in cancer diagnostics, therapeutics, theranostics and biomarker discovery: a comprehensive review. *Cancers*, *10*(2), 47.
40. Alkhamis, O., Canoura, J., Yu, H., Liu, Y., & Xiao, Y. (2019). Innovative engineering and sensing strategies for aptamer-based small-molecule detection. *TrAC Trends in Analytical Chemistry*, *121*, 115699.
41. Ruscito, A., & DeRosa, M. C. (2016). Small-Molecule Binding Aptamers: Selection Strategies, Characterization, and Applications. *Frontiers in chemistry*, *4*, 14.
42. Mannironi, C., Di Nardo, A., Fruscoloni, P., & Tocchini-Valentini, G. P. (1997). In vitro selection of dopamine RNA ligands. *Biochemistry*, *36*(32), 9726-9734.
43. Walsh, R., & DeRosa, M. C. (2009). Retention of function in the DNA homolog of the RNA dopamine aptamer. *Biochemical and biophysical research communications*, *388*(4), 732-735.
44. Nakatsuka, N., Yang, K. A., Abendroth, J. M., Cheung, K. M., Xu, X., Yang, H., ... & Andrews, A. M. (2018). Aptamer–field-effect transistors overcome Debye length limitations for small-molecule sensing. *Science*, *362*(6412), 319-324.
45. Kim, E., & Paeng, I. R. (2014). Advantageous sensitivity in the DNA homolog of the RNA dopamine aptamer. *Journal of Immunoassay and Immunochemistry*, *35*(1), 83-100.
46. Roth, A., & Breaker, R. R. (2009). The structural and functional diversity of metabolite-binding riboswitches. *Annual review of biochemistry*, *78*, 305-334.
47. Liu, X., He, F., Zhang, F., Zhang, Z., Huang, Z., & Liu, J. (2020). Dopamine and melamine binding to gold nanoparticles dominates their aptamer-based label-free colorimetric sensing. *Analytical chemistry*, *92*(13), 9370-93.

Chapter Two

Materials and Methods

2.1 Preparation of the MspA and variant proteins.

As described in the previous chapter, the experiments in this study were conducted with the MspA protein pore. Engineered MspA-M2, the mainstay of this study, was created through site directed mutagenesis which involved substituting six negatively charged amino acids (D and E) in the lumen of the wildtype MspA by neutral polar (N) and positively charged amino acids (R and K), specifically, D90N/D91N/D93N/D118R/D134R/E139K. In this study MspA-M2 was used as the model pore to study aptamer/ligand interactions. Additionally, MspA-M2 was used to construct variants at the R118 and R134 sites to probe the aptamer docking mechanism. The three M2-based variants are M2-R118N/R134N, M2-R118N and M2-R134N. henceforth the three variants are referred to as M3, M8 and M7.

The proteins of M2 and its variants were prepared as the method reported previously[1-4]. Briefly, the genes of M2 and variants with poly-histidine tag (H6) were inserted into the plasmid pET-30a(+) and cloned by GenScript Inc. Competent cells (*E. coli* BL21 (DE3)) were transformed with the plasmids by heat shock and then plated on LB agar supplemented with 50 μg/ml kanamycin. The plates were incubated at 37°C overnight. A single colony was picked and grew in 3ml LB medium with 50 μg/ml kanamycin and then was sub-cultured in 200ml same medium. When OD600=0.7~1.0, the cells were induced by 1 mM isopropyl β-D-thiogalactoside (IPTG) and shaken overnight at 16 °C. They were harvested by centrifugation at 4000 rpm 30 min at 4 °C in centrifuge tubes. The supernatant was discarded, and cell pellets were lysed in the lysis buffer (100 mM Na_2HPO_4/NaH_2PO_4, 0.1 mM EDTA, 150 mM NaCl, 0.5% (w/v) Genapol X-80 pH 6.5) at 60 °C for 10 min. The lysed cells were kept on ice for 10 min and centrifuged at

10,000 rpm 30 min at 4 °C. After syringe filtration through a 0.22 μm filter, the supernatant was transferred to a nickel affinity column (HisTrapTM HP, GE Healthcare). After washing the column by washing buffer (0.5 M NaCl, 20 mM HEPES, 5 mM imidazole, 0.5% (w/v) Genapol X-80, pH=8.0), the MspA mutants were eluted by using the elution buffer (500 mM imidazole, 0.5 M NaCl, 20 mM HEPES, 0.5% (w/v) Genapol X-80, pH=8.0). The elution aliquots (0.3~0.5 ml) with a gradient concentration of imidazole were sequentially collected in EP tubes. The assembly of MspA mutants was characterized by 12% SDS-PAGE. The aliquots with octamers were selected for the nanopore recording.

2.2 Aptamers and small molecule ligands.

The dopamine aptamers used in this study was published in Nakatsuka et al[5]. The sequence of the aptamer was CGACGCCAGTTTGAAGGTTCGTTCGCAGGTGTGGATGACGTCG. All the DNA fragments were synthesized by Integrated DNA Technologies, Inc. They were resolved in deionized water to 1 mM and diluted to 100 μM in 100 mM KCl, 20 mM Tris-Cl, pH 8.0 as the stock. Prior to use in the nanopore detection experiments, aptamers were denatured at 95 °C for 2 min, followed by cooling down gradually to room temperature overnight.

2.3 Nanopore single channel recording.

Nanopore single-channel recording was conducted in accordance with a previously reported protocol[7-8]. Briefly, a lipid bilayer membrane (1,2-diphytanoyl-sn-glycero-3-phosphocholine, Avanti Polar Lipids) was formed over a 100-150 μm orifice in the center of the Teflon film that created a partition between the cis and trans recording solutions. The solutions in both cis and trans chambers contained 1 M KCl buffered with 10 mM Tris (pH 7.4), unless otherwise stated. 100 nM of MspA proteins were added to the cis solution and stirred until they inserted into the bilayer to form a single nanopore channel. In many cases multiple channels

were formed. To cure this the bilayer was broken and formed again, followed by stirring of the cis solution. After a single nanopore channel was formed 100nM of the aptamer was added to the cis solution. This was followed by the addition of dopamine in the trans solution at desired concentrations. The voltage was applied from the trans solution, and the cis solution was grounded. The ionic current through the nanopore was recorded using an Axopatch 200B amplifier (Molecular Device Inc., Sunnyvale, CA), filtered with a built-in 4-pole low-pass Bessel Filter at 5 kHz, and acquired with Clampex 9/10 software (Molecular Device Inc.) through a Digidata 1440 A/D converter (Molecular Device Inc.) at a sampling rate of 20 kHz. Nanopore current trace analysis, including event duration histogram analysis and amplitude histogram analysis, were conducted using Clampfit 9/10 (Molecular Device Inc.), Excel (Microsoft) and SigmaPlot (SPSS) software. The nanopore experiments were performed at 22±2 °C. The result was presented as mean ± standard deviation ($n \geq 3$).

2.4 Artificial bilayer formation

Artificial phospholipid bilayer was formed on the orifice by the Montal-Mueller method which involved the following steps:

1. A fixed volume (1 ml) of buffer (1 M KCl [unless otherwise stated], 10 mM Tris, pH = 7.2,) is injected by a pipette into both cis and trans chambers.
2. Approximately 0.1 ml each of pretreat and lipid are added to the buffer on each side.
3. Five to ten minutes were given to the lipid to spread evenly and completely cover the liquid surface.
4. An additional 1 ml buffer was added on both sides, bringing up the lipid surface and forming a lipid bilayer through the orifice. The successful formation of a bilayer typically generates a square wave with a peak between150-200 pA, in response to a triangle -wave voltage applied at a frequency of 20Hz due to the capacitive property of the artificial membrane.

2.5 Nanopore insertion

Approximately 0.5 µl of 1µg/ml MspA is added into the cis chamber. This is followed by stirring the electrolyte in the cis chamber. Pore should insert within a matter of minutes. If pore does not insert after a few minutes more MspA is added to the cis. Too much MspA can lead to the insertion of many pores and make the trace difficult to analyze. Insertion of the pore is evidenced by the change of current from zero to a characteristic single pore current. If many pores are inserted, the chambers can be rinsed with fresh buffer. This is accomplished using two syringes. One syringe is used to withdraw electrolyte from the chamber while the other is simultaneously injecting a similar amount into the same chamber. Effectively this dilutes the MspA concentration.

2.6 Materials and General Methods

Reagents were purchased from the following suppliers and were of the highest purity available: oligonucleotides were purchased from Integrated DNA Technologies (Coralville, IA).

Dopamine was purchased from Sigma Inc (St. Louis, MO).

All chemicals, including KCl, NaC, LiCl, CaCl2 and MgCl2 were purchased from Sigma-Aldrich (St. Louis, MO).

1,2-diphytanoylsn-glycero-3-phosphocholine (DPhPC) lipid was obtained from Avanti Polar Lipids (U.S.A.).

The thickness of Teflon film (Goodfellow) was 25 µm.

The surface of the membrane surrounding the aperture was pre-treated to increase its affinity to lipids. The membrane was pre-treated with long chain organic molecules (hexadecane) in an organic solvent (pentane). The proportion of the hexadecane to the pentane in the pretreat was

1:10 volume to volume. The volume of hexadecane in pentane used is typically from 0.1µl to l0µl.

Each set of nanopore experiments was run several times.

2.7 Data processing and analysis

An Axopatch 200B was used to record and amplify the pico-ampere current through the pore. The initial recordings were then filtered with a built-in 4-pole low-pass Bessel filter at 5 kHz, and finally captured and converted by DigiData 1440A A/D converter into the computer at 20 kHz sampling rate. The entire process was monitored and controlled through an on-board Clampex 10.4 system. Analysis of the recorded trace, including amplitude histogram analysis and duration histogram analysis, was performed using Clampfit 10.7. (All equipment and software used above were purchased from Molecular Devices Inc., Sunnyvale, CA, USA).

The mean dwell time τoff and the mean binding time τon were obtained from the trace histograms by fitting the distributions to a single exponential function. The association rate constant, kon, was obtained by the equation kon = 1/ (τon[DNA]), where τon is the mean binding time and [DNA] is the concentration of ssDNA in solution. The dissociation rate constant, koff, was calculated using the equation koff = 1/τoff, where τoff is the mean dwell time of ssDNA in the nanopore.

Results were presented in mean ± standard deviation.

Data from several experiments were pooled together and bootstrapping techniques were employed using r software to check for concordance with the mean and standard deviation obtained from the histograms.

References

1. Yan, S., Li, X., Zhang, P., Wang, Y., Chen, H. Y., Huang, S., & Yu, H. (2019). Direct sequencing of 2′-deoxy-2′-fluoroarabinonucleic acid (FANA) using nanopore-induced phase-shift sequencing (NIPSS). *Chemical science*, *10*(10), 3110-3117.

2. Wang, Y., Yan, S., Zhang, P., Zeng, Z., Zhao, D., Wang, J., ... & Huang, S. (2018). Osmosis-driven motion-type modulation of biological nanopores for parallel optical nucleic acid sensing. *ACS applied materials & interfaces*, *10*(9), 7788-7797.

3. Heinz, C., Karosi, S., & Niederweis, M. (2003). High-level expression of the mycobacterial porin MspA in Escherichia coli and purification of the recombinant protein. *Journal of Chromatography B*, *790*(1-2), 337-348.

4. Butler, T. Z., Pavlenok, M., Derrington, I. M., Niederweis, M., & Gundlach, J. H. (2008). Single-molecule DNA detection with an engineered MspA protein nanopore. *Proceedings of the National Academy of Sciences*, *105*(52), 20647-20652.

5. Nakatsuka, N., Yang, K. A., Abendroth, J. M., Cheung, K. M., Xu, X., Yang, H., ... & Andrews, A. M. (2018). Aptamer–field-effect transistors overcome Debye length limitations for small-molecule sensing. *Science*, *362*(6412), 319-324.

6. Jenison, R. D., Gill, S. C., Pardi, A., & Polisky, B. (1994). High-resolution molecular discrimination by RNA. *Science*, *263*(5152), 1425-1429.

7. Wang, Y., Zheng, D., Tan, Q., Wang, M. X., & Gu, L. Q. (2011). Nanopore-based detection of circulating microRNAs in lung cancer patients. *Nature nanotechnology*, *6*(10), 668-674.

8. Tian, K., Chen, X., Luan, B., Singh, P., Yang, Z., Gates, K. S., ... & Gu, L. Q. (2018). Single locked nucleic acid-enhanced nanopore genetic discrimination of pathogenic serotypes and cancer driver mutations. *ACS nano*, *12*(5), 4194-4205.

Chapter Three

Real-time Detection of Dopamine – Aptamer Interactions in a Nanopore.

3.1 Introduction

Rapid and label-free detection of small molecules is a compelling goal in diagnostics, synthetic biology, and drug discovery where it has broad applications. Several methods have been developed to this end. These include, ultrahigh performance liquid chromatography mass spectroscopy, electrochemistry, positron emission tomography scanning, fluorescent enzyme-based biosensors, micro-dialysis, and field-effect (FET) transistors. Each of these methods has inherent drawbacks. Although mass spectroscopy and liquid chromatography instrumentation is widely available and yields impressive results, the process is too slow and cumbersome. Hence it is not suitable for real time detection and monitoring of small molecules. Micro-dialysis suffers from poor temporal resolution. The utility of electrochemical approaches is limited in the analysis of samples that contain analogues and interferents. For instance, the presence of dopamine analogues such as norepinephrine, epinephrine, L-Dopa, D-tyrosine, L-tyrosine and tyramine as well as interferents such as uracil and uric acid, complicate the detection of dopamine by electrochemical methods[2]. Positron emission tomography scanning requires the injection of trace amounts of radioactive substances into the subject. Subjects are often wary of exposure to radiation. FET-based biosensors have desirable characteristics, such as rapid label-free electrical detection, low power consumption, portability, inexpensive mass production, and the possibility of on-chip integration of both sensor and measurement systems but suffer from poor stability and selectivity[3-5]. Additionally, obstructions from the Debye length weaken the FET signal. Poor signals are also produced with low and uncharged ligands. Furthermore, FET is not a single molecule detection system[6].Enzymatic based sensors are associated with high cost,

complicated production procedures, and short shelf lives[7]. Aptamer-based sensors do not suffer from these drawbacks. Aptamer based biosensors can be grouped into three broad groups- fluorescent, calorimetric and electrochemical. Aptamer based fluorescent aptamers are susceptible to photobleaching which limits their longevity. Both the fluorescent based, and calorimetric based aptamers must be mixed with the sample to be analyzed[3].

This is a limitation because the tertiary structures of aptamers are highly dependent on solution conditions. Moreover, aptamers easily degrade when mixed with biological fluids. Electrochemical-based aptamer sensors must overcome the challenge posed by analogues and interferents. Nanopore-based aptamer sensors are free of these limitations since the aptamer and the sample are in different compartments. The current work presents a versatile aptamer-based nanopore sensing platform capable of small molecule detection and measurement, drug screening and conformation analysis.

Aptamers are single-stranded nucleic acids that can bind target molecules with high affinity and specificity[8]. Various nucleic acid aptamers have been generated and used to detect biologically important small molecules, including neurotransmitters, hormone, metabolites, antibiotics and anticancer drugs, for biological mechanism exploration, disease diagnostics, enzyme profiling and pharmacokinetics study[9-12]. The aptamer can fold into a tertiary scaffold, and the ligand binding can change the aptamer conformation, a sensor can be used to discriminate different conformations of an aptamer molecule, and by analyzing the dynamic conversion between different aptamer conformations, quantify the target small molecule.

Moreover, understanding small-molecule regulation of nucleic acid conformation is important to reveal biological mechanisms and to develop biotechnological applications. For example, native regulatory nucleic acids such as riboswitches control gene expression via a conformational

transition upon binding with metabolites[1], serving as new targets for antibiotic design[2-3]. New therapeutic compounds can be discovered by screening small molecules that bind the target nucleic acid motifs, change their conformation, and modulate their biological functions[4-11]. Furthermore, *in vitro* selected nucleic acid aptamers and engineered riboswitches[12-14] can change their conformation upon ligand binding. Utilizing this property, biosensors can be designed to detect biologically important small molecules, including neurotransmitters[14-19] and hormones[20], metabolites[12-13, 21], antibiotics[22] and anticancer drugs[23], for biological mechanism exploration, disease diagnostics, enzyme profiling and pharmacokinetics studies. In addition, small molecule-sensing aptamers, such as the theophylline aptamer, can be engineered into gene circuits[24-27], and activated through a ligand-triggered conformational transition to program gene expression and gene editing[27-28]. To advance the use of nucleic acids as sensors, development of sensitive, fast and low-cost tools is needed that can discriminate different conformations of single nucleic acid molecules and reveal their dynamic transitions in response to small-molecule binding.

Nanopore single-molecule-based biosensing techniques have been applied to sequencing[29-36] and various genetic[37-38], epigenetic[39-45] and proteomic[46-50] analyses. By measuring dynamic changes of current through the nanopore, this technique has also demonstrated great potential to detect biomolecular structures. When a protein[51], DNA[30, 52-53], RNA[54,55] or nucleic acid/protein complex[56-57] occludes the nanopore under a transmembrane voltage, their structure can characteristically modulate the ion current through the pore. The resulting nanopore current pattern or signature can be analyzed to discriminate the molecular structure[58-62]. However, these nanopore measurements to study biomolecular structure are often limited to providing a conformational 'snapshot', and do not reveal dynamic conformational variation of each molecule detected. This limitation can be overcome by engineering or attaching

a nucleic acid or polypeptide probe to the nanopore to detect reversible binding of a protein ligand[63-65]. Such approaches are generally not sensitive enough to detect small conformational changes of a nucleic acid scaffold upon the binding of a small ligand. In addition, fabrication of a nanopore with an attached molecular probe can be complicated. Recently, the ClyA protein pore has been used to trap a protein molecule in its large cylinder cavity, enabling the nanopore to elucidate protein-protein interactions[66] and detect protein-binding metabolites[67-69]. This study presents a new strategy for label-free detection of biomolecular conformational changes confined in a large nanopore.

This work presents a label-free aptamer-inlaid nanopore capable of pinpointing small molecule-induced single nucleic acid molecule conformational variations (Fig. 1). The MspA protein pore has been developed for sequencing[42, 70-73], biomolecular mechanistic study[74] and single-molecule chemistry[75]. This goblet-shaped nanopore encloses a 3-5 nm wide cavity in the cis vestibule. It is demonstrated that an aptamer can be stably docked in this confinement via coordination to a positive charge ring (R118) in the lumen. This docking configuration enables the nanopore to discriminate conformational transitions of the aptamer as it binds and releases single ligand molecules.

Dopamine and serotonin binding aptamers are employed as testbeds to validate this sensor platform. By analyzing aptamer conformational changes, the target neurotransmitter concentration can be quantified. Moreover, different neurotransmitters can be distinguished based on their characteristic aptamer-ligand interactions. Thus, offering the potential to build a modular nanopore toolbox for dynamic detection of multiple ligands. This sensor platform can detect rapid conformation change of nucleic acid with a temporal resolution of 1ms, with no need for aptamer-ligand binding to reach equilibrium. This sensor platform can be adapted for

therapeutic compound discovery by screening small molecules for DNA/RNA interactions and artificial riboswitch design by evaluating ligand-triggered nucleic acid conformational changes.

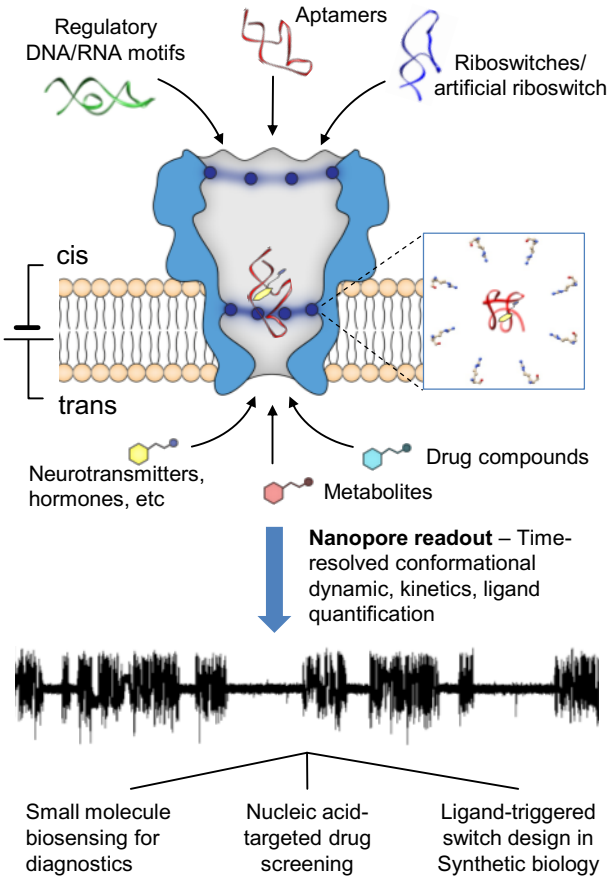

Fig 3. 1: Principle and applications of a nanopore sensor capable of discriminating nucleic acids conformational transitions in response to small-molecule binding.

A nucleic acid receptor is docked in a MspA protein pore from one side (cis), and its small molecule ligand can enter the pore from the opposite side (trans) to bind the docked receptor. The induced nucleic acid conformational change upon ligand binding characteristically modulates the nanopore ion current, allowing use of the current signature to resolve dynamic transitions between different conformations. By analyzing conformational variation, the sensor platform can be adapted to detect biologically important small molecules such as neurotransmitters and hormones, and screen nucleic acid-small molecule interactions for drug discovery and synthetic biology design.

3.2. Methods

The Materials and Methods are described in chapter two.

3.3 Results

3.3.1 Dopamine-induced aptamer conformational transitions in the nanopore

MspA forms an octameric protein nanopore in the lipid bilayer. In this study the mutant M2 pore that has been developed for sequencing and biomolecular detection was used. A dopamine-binding aptamer was added to the cis solution. Driven by a transmembrane potential of +180 mV, the aptamer produced a transient current block with a duration of τ_A=1.02±0.19s (Fig.3. 2a and d). Its blocking level rapidly transitioned between two states, A1 at I/I_0=53.0 ± 0.3% and A2 at I/I_0=47.6 ± 0.4% (Fig.3. 2a). This signature pattern reveals that the aptamer is captured by the nanopore from the cis entrance and stably lodged in the nanopore lumen. The aptamer rapidly transitions between two conformations, which modulate the nanopore current between the two levels. The aptamer finally unfolds and translocates through the pore, resulting in the transient, highly blocked level, A3.

Dopamine was then added to the trans solution. The trans dopamine was isolated from the cis aptamer by the membrane but could interact with the aptamer within the pore. Addition of trans dopamine immediately generated a new, stable single-level signature, AL, with a blocking level at I/I_0=49.5±0.5% and a duration of τ_{off}=152±18 ms (Fig.3. 2b, marked by red lines). The frequency of the AL blocks *f* was calculated from the inter-block interval τ_{on} (f=1/τ_{on}). *f* was monotonically increased with the addition of dopamine, from 1.2±0.2 s^{-1} in 5 μM dopamine to 9.7±0.4 s^{-1} in 100 μM dopamine (Fig. 2b and e). These findings together suggest that the AL blocks should be generated by the aptamer in the dopamine-bound conformation. The nanopore can discriminate it from dopamine-free aptamer conformations based on the blocking level variation. As such, the entire nanopore signature records a series of aptamer conformational transitions as single dopamine molecules are bound and released.

To quantify aptamer-dopamine interactions (Fig.3. 2f and g), transitions among different aptamer conformations from their nanopore blocking levels were identified. The aptamer signature (Fig.3. 2b, expanded trace) reveals the following kinetic pathway: The aptamer without dopamine binding can rapidly transition between two conformations A1 and A2. Only A2 can transition to the dopamine-bound conformation AL, and there is no connection between A1 and AL, suggesting that dopamine only selectively bind to the A2 conformation. The dopamine-bound aptamer (AL) increases the blocking level from A2. Upon dopamine dissociation, the aptamer transitions back to A2, which then rapidly transitions between the A2 and A1 states, while waiting for the binding of the next dopamine molecule. In this pathway, the transition rates between free aptamer A1 and A2 were $k_{A1\rightarrow A2}$=91±18 s^{-1} and $k_{A2\rightarrow A1}$=125±13 s^{-1}, calculated from the lifetimes of A1 (τ_{A1}=11±2 ms) and A2 (τ_{A2}=8±1 ms); The apparent association rate constant for aptamer•dopamine was k_{on}'=0.16±0.02 $\mu M^{-1}\cdot s^{-1}$ (25 μM dopamine, Fig. 3.2f), calculated by $k_{on}^{'} = \frac{1}{\tau_{on}[L]}$ (Eq. S4) and its dissociation rate constant was k_{off}=6.6±0.8 s^{-1} (Fig. 2g), calculated by $k_{off}=1/\tau_{off}$ (Eq. S2). In addition, the binding of dopamine considerably increased the aptamer residence time in the nanopore, τ_A, from 1.02±0.19 s to 1.90±0.29 s (Fig. 3.2d), suggesting that the dopamine binding stabilizes the aptamer structure in the pore.

3.3.2 Dopamine aptamer selectivity

To understand the mechanism for the dopamine aptamer ligand selectivity, the interactions of the aptamer with chemically related neurotransmitters (Fig.3. 2c) were screened. Both serotonin and norepinephrine sporadically bound to the dopamine aptamer at much lower frequencies (f=0.022 s^{-1} and 0.034 s^{-1}, respectively, at 50 μM), resulting in 300- and 260-fold lower association rate constants compared with dopamine (Fig. 3.2f). In contrast to the frequency, the duration of the serotonin and norepinephrine binding events (τ_{off}=63 ms and 47

ms) were moderately shorter than dopamine (τ_{off}=157 ms), suggesting 2.5-fold (serotonin) and 3-fold (norepinephrine) higher dissociation rate constants (Fig.3. 2g). Such high ligand selectivity is primarily determined by the fast association rate for dopamine, which forms a $\Delta\Delta G$=3.3-3.8 kcal·mol^{-1} barrier to prevent binding of non-dopamine neurotransmitters (Eq. S5).

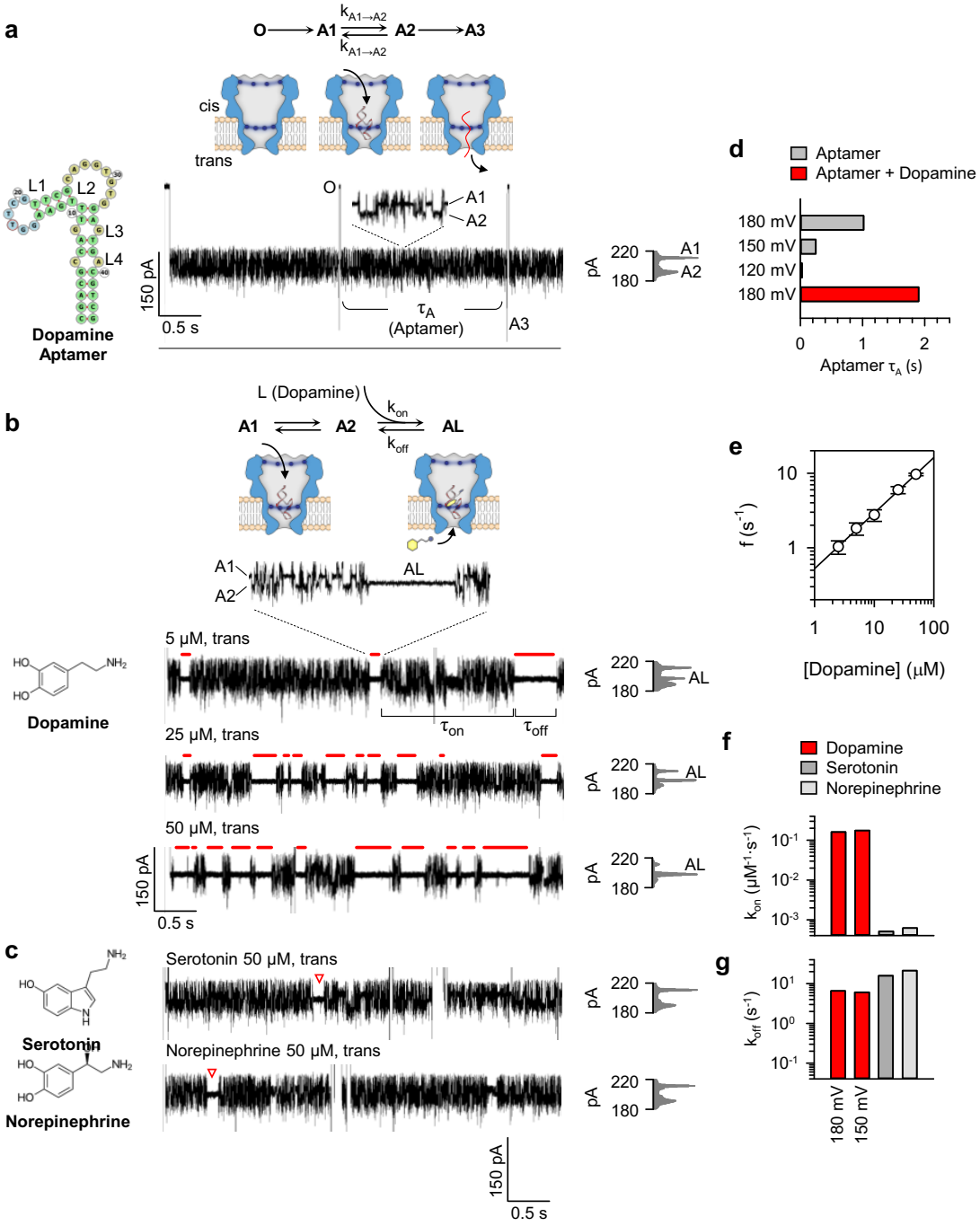

Fig 3. 2: Detection of dopamine by discriminating the dopamine aptamer conformational changes in the MspA protein pore.

a. Kinetic model, nanopore current signatures and current blocking level histograms showing the capture of an aptamer into the nanopore, transitions between aptamer conformations (A1 and A2), and unfolding-translocation of the aptamer (A3) after long-time residence in the pore; **b.** Single pore current signatures showing dopamine binding event, i.e., dopamine-bound aptamer conformation (AL, marked by red lines) at different dopamine concentrations, and the kinetic pathway for aptamer-dopamine interaction; **c.** Single pore current signatures for binding of serotonin (upper panel) and norepinephrine (lower panel) to the dopamine aptamer; **d.** Aptamer residence time (τ_A) in the absence (180, 150, 120 mV) and in the presence of dopamine (180 mV); **e.** Frequency of dopamine binding events as a function as the dopamine concentration; **f** and **g.** Association rate constant (k_{on}, f) and dissociation rate constant (k_{off}, g) for binding of the dopamine aptamer with 25 μM dopamine (180 mV/150 mV), 25 μM serotonin (120 mV), and 25 μM norepinephrine (180 mV). The nanopore was recorded in 1 M KCl and 10 mM Tris (pH7.4), with 100 nM aptamer in cis solution and different concentrations of dopamine in the trans solution.

3.3.4 Docking a dopamine aptamer with a cationic ring engineered in the MspA nanopore

The nanopore's sensitivity to the aptamer conformations originates from its lodging configuration in the nanopore. To understand where and how the aptamer interacts with the nanopore, a group of mutant pores with selectively altered charge distribution in the nanopore lumen were constructed through site directed mutagenesis. The candidate aptamer locations in the M2 pore include the R118 ring in the middle of the pore and the R134 ring near the cis entrance[76] (Fig.3. 3a). First to be tested was the mutant M2-R118N/R134N pore, which replaces both R118 and R134 rings with neutral asparagine (Fig. 3b model). With this mutant the aptamer in the cis compartment no longer produced the M2-like prolonged block at 180 mV (Fig.3. 3b, left trace), but only short-lived partial blocks (I/I_0=61.2±0.9%, τ_A=1.4±0.4 ms), indicating that the nanopore without both positive charge rings cannot capture the aptamer. Next to be tested was the mutant M2-R118N pore, which removes the R118 ring but retains the R134 ring (Fig.3. 3c model). Still, there were no prolonged blocking events observed (Fig. 3c, left trace) and the aptamer only produced short-lived blocks (I/I_0=60.7±0.8%, τ_A=0.7±0.3 ms). As neither pore can capture the aptamer, it is unsurprising that there were no dopamine binding events from the trans solution (Fig. 3b and c, right traces). It is hypothesized that the aptamer enters the nanopore and

traverses all the way to R118N, but in the absence of the positive charge it is not captured and therefore eventually exists back to the cis side. Alternatively, it rapidly translocated through to the trans side at such a fast velocity that translocation duration (<1 μs) is so brief that the event cannot be captured by the instrument. This phenomenon can be explained by the presence of a high biasing voltage (180mV).

Lastly the mutant M2-R134N pore, which retains the R118 ring but removes the R134 ring (Fig.3. 3d model) was tested. Interestingly, this pore completely recapitulates the functional interactions with the aptamer found in the native M2 pore. The aptamer generated the M2-like blocking signatures (Fig.3. 3d, left), which feature long residence time (τ_A=1.5±0.2 s) and rapid transitions between two conformations A1 (I/I_0=50.7±0.6%) and A2 (I/I_0=47.9±1.0%) ($k_{A1\rightarrow A2}$=79±19 s^{-1} and $k_{A2\rightarrow A1}$=113±15 s^{-1}). Dopamine can also bind the aptamer in the pore from the trans side (Fig. 3d, right trace, marked by red lines), with similar kinetics (k_{on}=0.14±0.03 $\mu M^{-1}\cdot s^{-1}$ and k_{off}=4.9±0.7 s^{-1}). Therefore, by screening the nanopore charge distribution, it is concluded that the R118 ring plays a key role in capturing and docking the dopamine aptamer, whereas the R134 ring does not contribute significantly to the pore's interactions with the aptamer. The aptamer docked in this location is likely coordinated by the surrounding eight arginine residues. It is this docking mechanism that enables the nanopore to stably trap the aptamer, and to be sensitive enough to discriminate different aptamer conformations.

In summary, based on the M2, M3, M7 and M8 results taken together, the aptamer should be pulled through all the charged rings at the cis entrance, migrate all the way down to the R118 ring in the middle of the pore where it is embedded in a charged field layer generated by his ring and immobilized by coordination with the surrounding eight arginine residues.

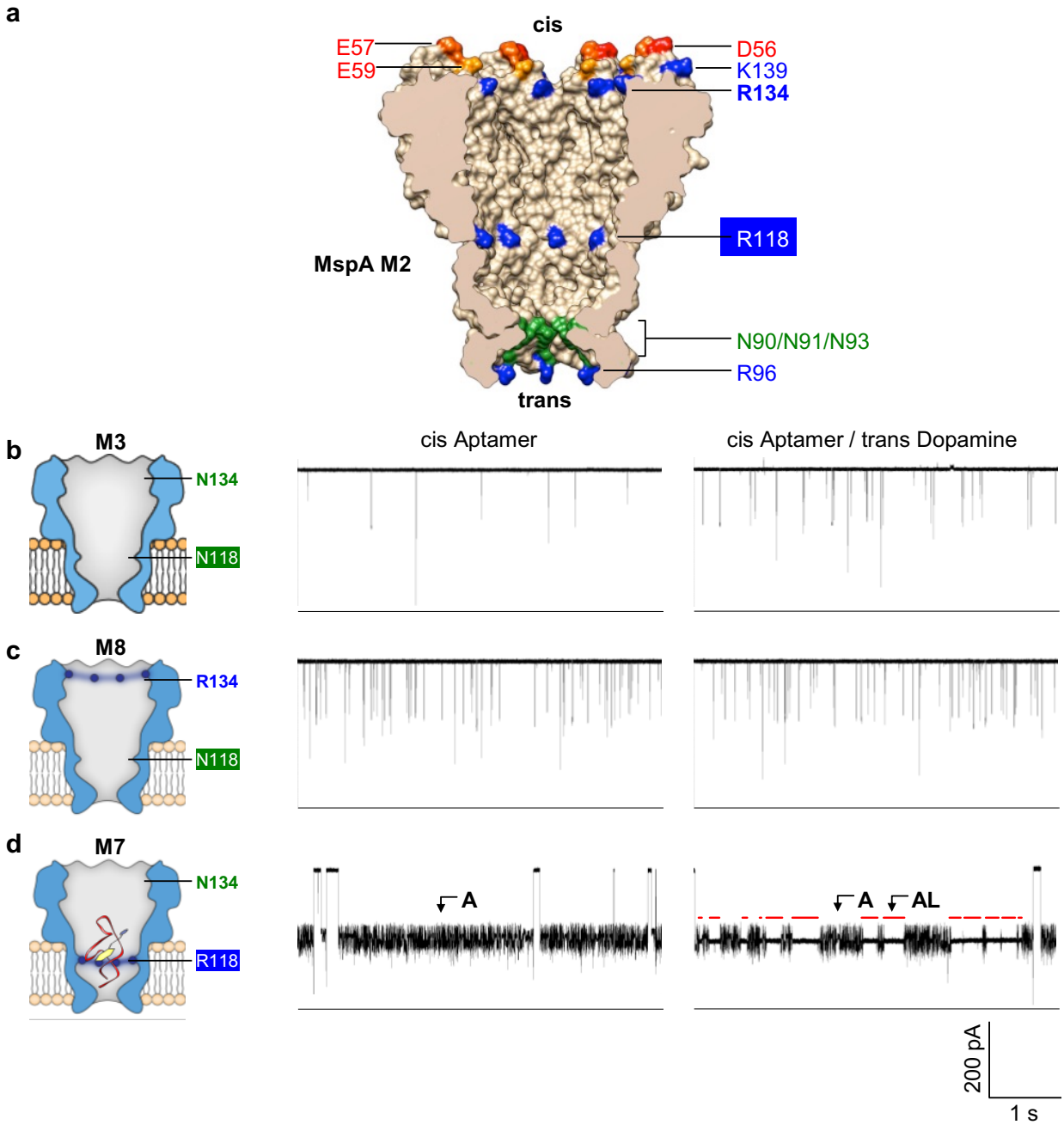

Fig 3. 3: Understanding the aptamer docking mechanism in the MspA pore by changing charge distribution in the lumen.

a. Structure of the MspA-M2 protein pore. Positively (blue) and negatively (red) charged amino acid residues in the lumen are marked. The aptamer docking site at the R118 ring is highlighted; **b-d.** Charge-altering mutations in the M2 pore were made, including M2-R118N/R134N (b), M2-R118N (c) and M2-R134N (d), and corresponding single-pore current signatures for the dopamine aptamer in the absence (left) and presence (right) of dopamine. The

nanopore was recorded at +180 mV in 1 M KCl and 10 mM Tris (pH7.4), with 100 nM aptamer variants in the cis solution and 25 μM dopamine in the trans solution.

3.4 Discussion

The aptamer-inlaid nanopore can discriminate conformational changes in single nucleic acid molecules in response to small-molecule binding, offering a novel sensor platform for both sensitive and selective small-molecule biosensing. To build this sensor platform, the nanopore used should possess a cavity in the conductive pathway large enough to accommodate the target nucleic acid structure. For example, the dopamine experiments demonstrated that the MspA's nanopore cavity can contain a 50-nt functional nucleic acid scaffold. Another requirement is that the nanopore ionic current should characteristically vary in response to nucleic acid conformational changes that occur upon ligand binding, thus being able to continuously report conformational transitions as the ligand binds and unbinds.

The neurotransmitter detection experiments (Fig.3.2) reveal that, by reading the aptamer conformations from specific current-block fingerprints, the target ligand can be successfully discriminated from non-target species. Thus, making ultra-sensitive small molecule detection and discrimination possible.

3.5 Limitations

Further development is needed to overcome the challenges to practical applications. For example, the aptamer capture by the MspA pore (M2 and M7) is disabled at low salt concentrations (data not shown). This limitation must be overcome for neurotransmitter detection in physiological extracellular solutions such as artificial cerebrospinal fluid (aCSF, ~150 mM salt).

3.6 Conclusion.

Understanding how small-molecule ligands regulate nucleic acid structures is important in both bio-mechanism elucidation and biotechnological applications. Conformational changes in naturally occurring nucleic acid motifs that result from ligand binding can be used to screen therapeutic compounds; *In vitro* selected aptamers can be used to detect small molecule biomarkers, and ligand-triggered riboswitches can be designed to control gene expressions. Here we propose a label-free and modular aptamer-inlaid nanopore capable of revealing time-resolved single nucleic acid molecule conformational transitions with millisecond resolution in response to small molecule ligand binding. By analyzing single nucleic acid molecule conformational transitions, the sensor platform can be adapted to detect biologically important small molecules such as neurotransmitters for neurochemistry exploration, and screen nucleic acid-small molecule interactions for nucleic acid-targeted drug discovery and synthetic biology design.

Chapter four will present efforts to enhance the sensitivity of detection and measurement of dopamine.

References

1.McCown, P. J.; Corbino, K. A.; Stav, S.; Sherlock, M. E.; Breaker, R. R. (2017). Riboswitch Diversity and Distribution. *RNA***,** *23*, 995-1011.

2.Reyes-Darias, J. A.; Krell, T. (2017) Riboswitches as Potential Targets for the Development of Anti-Biofilm Drugs. *Curr Top Med Chem, 17*, 1945-1953.

3.Aghdam, E. M.; Hejazi, M. S.; Barzegar, A. (2016). Riboswitches: From Living Biosensors to Novel Targets of Antibiotics. *Gene, 592*, 244-259.

4.Warner, K. D.; Hajdin, C. E.; Weeks, K. M. (2018). Principles for Targeting Rna with Drug-Like Small Molecules. *Nat. Rev. Drug Discov, 17*, 547-558.

5.Donlic, A.; Hargrove, A. E.(2018). Targeting Rna in Mammalian Systems with Small Molecules. *Wiley interdisciplinary reviews. RNA,9*, e1477.

6.Howe, J. A.; Wang, H.; Fischmann, T. O.; Balibar, C. J.; Xiao, L.; Galgoci, A. M.; Malinverni, J. C.; Mayhood, T.; Villafania, A.; Nahvi, A.; Murgolo, N.; Barbieri, C. M.; Mann, P. A.; Carr, D.; Xia, E.; Zuck, P.; Riley, D.; Painter, R. E.; Walker, S. S.; Sherborne, B., et al.(2015). Selective Small-Molecule Inhibition of an Rna Structural Element. *Nature, 526*, 672-677.

7.Childs-Disney, J. L.; Disney, M. D. (2016). Approaches to Validate and Manipulate Rna Targets with Small Molecules in Cells. In *Annual Review of Pharmacology and Toxicology, Annual Reviews Inc,56*,123-140.

8.Parsons, J.; Castaldi, M. P.; Dutta, S.; Dibrov, S. M.; Wyles, D. L.; Hermann, T. (2009). Conformational Inhibition of the Hepatitis C Virus Internal Ribosome Entry Site Rna. *Nature chemical biology, 5*, 823-825.

9.Wang, J.; Schultz, P. G.; Johnson, K. A. (2018). Mechanistic Studies of a Small-Molecule Modulator of Smn2 Splicing. *Proceedings of the National Academy of Sciences of the United States of America, 115*, E4604-E4612.

10.Hilimire, T. A.; Chamberlain, J. M.; Anokhina, V.; Bennett, R. P.; Swart, O.; Myers, J. R.; Ashton, J. M.; Stewart, R. A.; Featherston, A. L.; Gates, K.; Helms, E. D.; Smith, H. C.; Dewhurst, S.; Miller, B. L. (2017). Hiv-1 Frameshift Rna-Targeted Triazoles Inhibit Propagation of Replication-Competent and Multi-Drug-Resistant Hiv in Human Cells. *ACS Chem. Biol,12*, 1674-1682.

11.Hermann, T.(2016). Small Molecules Targeting Viral Rna. *Wiley Interdiscip. Rev. RNA, 7*, 726-743.

12.Su, Y.; Hickey, S. F.; Keyser, S. G.; Hammond, M. C. (2016). In Vitro and in Vivo Enzyme Activity Screening Via Rna-Based Fluorescent Biosensors for S-Adenosyl-L-Homocysteine (Sah). *Journal of the American Chemical Society, 138*, 7040-7047.

13.You, M.; Litke, J. L.; Jaffrey, S. R. (2015). Imaging Metabolite Dynamics in Living Cells Using a Spinach-Based Riboswitch. *Proceedings of the National Academy of Sciences of the United States of America,112*, E2756-E2765.

14.Porter, E. B.; Polaski, J. T.; Morck, M. M.; Batey, R. T. (2016). Recurrent Rna Motifs as Scaffolds for Genetically Encodable Small-Molecule Biosensors. *Nature chemical biology,13*, 295-301.

15.Nakatsuka, N.; Yang, K. A.; Abendroth, J. M.; Cheung, K. M.; Xu, X.; Yang, H.; Zhao, C.; Zhu, B.; Rim, Y. S.; Yang, Y.; Weiss, P. S.; Stojanovic, M. N.; Andrews, A. M. (2018). Aptamer-Field-Effect Transistors Overcome Debye Length Limitations for Small-Molecule Sensing. *Science,362*, 319-324.

16.Saraf, N.; Bosak, A.; Willenberg, A.; Das, S.; Willenberg, B. J.; Seal, S. (2017). Colorimetric Detection of Epinephrine Using an Optimized Paper-Based Aptasensor. *RSC Advances, 7*, 49133-49143.

17.Chavez, J. L.; Hagen, J. A.; Kelley-Loughnane, N. (2017). Fast and Selective Plasmonic Serotonin Detection with Aptamer-Gold Nanoparticle Conjugates. *Sensors, 17*.

18.Walsh, R.; DeRosa, M. C. (2009). Retention of Function in the DNA Homolog of the Rna Dopamine Aptamer. *Biochemical and biophysical research communications, 388*, 732-735.

19.Mannironi, C.; Di Nardo, A.; Fruscoloni, P.; Tocchini-Valentini, G. P. (1997). In Vitro Selection of Dopamine Rna Ligands. *Biochemistry,36*, 9726-9734.

20.Liang, S.; Kinghorn, A. B.; Voliotis, M.; Prague, J. K.; Veldhuis, J. D.; Tsaneva-Atanasova, K.; McArdle, C. A.; Li, R. H. W.; Cass, A. E. G.; Dhillo, W. S.; Tanner, J. A. (2019). Measuring Luteinising Hormone Pulsatility with a Robotic Aptamer-Enabled Electrochemical Reader. *Nature communications,10*, 852.

21.Tapsin, S.; Sun, M.; Shen, Y.; Zhang, H.; Lim, X. N.; Susanto, T. T.; Yang, S. L.; Zeng, G. S.; Lee, J.; Lezhava, A.; Ang, E. L.; Zhang, L. H.; Wang, Y.; Zhao, H.; Nagarajan, N.; Wan, Y. (2018). Genome-Wide Identification of Natural Rna Aptamers in Prokaryotes and Eukaryotes. *Nature communications, 9*.

22.Mehlhorn, A.; Rahimi, P.; Joseph, Y. (2018). Aptamer-Based Biosensors for Antibiotic Detection: A Review. *Biosensors,8*.

23.Li, H.; Dauphin-Ducharme, P.; Arroyo-Currás, N.; Tran, C. H.; Vieira, P. A.; Li, S.; Shin, C.; Somerson, J.; Kippin, T. E.; Plaxco, K. W. (2017). A Biomimetic Phosphatidylcholine-Terminated Monolayer Greatly Improves the in Vivo Performance of Electrochemical Aptamer-Based Sensors. *Angew. Chem. Int. Ed.,56*, 7492-7495.

24.Wrist, A.; Sun, W.; Summers, R. M. (2020).The Theophylline Aptamer: 25 Years as an Important Tool in Cellular Engineering Research. *ACS Synth Biol,9*, 682-697.

25.Soukup, G. A.; Breaker, R. R.(1999). Engineering Precision Rna Molecular Switches. *Proceedings of the National Academy of Sciences of the United States of America, 96*, 3584-3589.

26.Jenison, R. D.; Gill, S. C.; Pardi, A.; Polisky, B. (1994).High-Resolution Molecular Discrimination by Rna. *Science, 263*, 1425-1429.

27.Kundert, K.; Lucas, J. E.; Watters, K. E.; Fellmann, C.; Ng, A. H.; Heineike, B. M.; Fitzsimmons, C. M.; Oakes, B. L.; Qu, J.; Prasad, N.; Rosenberg, O. S.; Savage, D. F.; El-Samad, H.; Doudna, J. A.; Kortemme, T. (2019). Controlling Crispr-Cas9 with Ligand-Activated and Ligand-Deactivated Sgrnas. *Nature communications,10*, 2127.

28.Lin, B.; An, Y.; Meng, L.; Zhang, H.; Song, J.; Zhu, Z.; Liu, W.; Song, Y.; Yang, C. (2019). Control of Crispr-Cas9 with Small Molecule-Activated Allosteric Aptamer Regulating Sgrnas. *Chem Commun (Camb),55*, 12223-12226.

29.Clarke, J.; Wu, H.-C.; Jayasinghe, L.; Patel, A.; Reid, S.; Bayley, H. (2009). Continuous Base Identification for Single-Molecule Nanopore DNA Sequencing. *Nat. Nano,4*, 265-270.

30.Cherf, G. M.; Lieberman, K. R.; Rashid, H.; Lam, C. E.; Karplus, K.; Akeson, M. (2012). Automated Forward and Reverse Ratcheting of DNA in a Nanopore at 5-a Precision. *Nat. Biotechnol.,30*, 344-348.

31.Manrao, E. A.; Derrington, I. M.; Laszlo, A. H.; Langford, K. W.; Hopper, M. K.; Gillgren, N.; Pavlenok, M.; Niederweis, M.; Gundlach, J. H. (2012). Reading DNA at Single-Nucleotide Resolution with a Mutant Mspa Nanopore and Phi29 DNA Polymerase. *Nat. Biotechnol.* **2012,** *30*, 349-353.

32.Laszlo, A. H.; Derrington, I. M.; Ross, B. C.; Brinkerhoff, H.; Adey, A.; Nova, I. C.; Craig, J. M.; Langford, K. W.; Samson, J. M.; Daza, R.; Doering, K.; Shendure, J.; Gundlach, J. H. (2014). Decoding Long Nanopore Sequencing Reads of Natural DNA. *Nat. Biotechnol,32*, 829-833.

33.Jain, M.; Fiddes, I. T.; Miga, K. H.; Olsen, H. E.; Paten, B.; Akeson, M. (2015). Improved Data Analysis for the Minion Nanopore Sequencer. *Nature methods,12*, 351-356.

34. Fuller, C. W.; Kumar, S.; Porel, M.; Chien, M.; Bibillo, A.; Stranges, P. B.; Dorwart, M.; Tao, C.; Li, Z.; Guo, W.; Shi, S.; Korenblum, D.; Trans, A.; Aguirre, A.; Liu, E.; Harada, E. T.; Pollard, J.; Bhat, A.; Cech, C.; Yang, A., et al. (2016). Real-Time Single-Molecule Electronic DNA Sequencing by Synthesis Using Polymer-Tagged Nucleotides on a Nanopore Array. *Proc. Natl. Acad. Sci. USA,113*, 5233-5238.

35.Kim, D.; Lee, J. Y.; Yang, J. S.; Kim, J. W.; Kim, V. N.; Chang, H. (2020).The Architecture of Sars-Cov-2 Transcriptome. *Cell,181*, 914-921

36.Van der Verren, S. E.; Van Gerven, N.; Jonckheere, W.; Hambley, R.; Singh, P.; Kilgour, J.; Jordan, M.; Wallace, E. J.; Jayasinghe, L.; Remaut, H. (2020). A Dual-Constriction Biological

Nanopore Resolves Homonucleotide Sequences with High Fidelity. *Nat Biotechnol,38*, 1415-1420.

37.Cao, C.; Ying, Y.-L.; Hu, Z.-L.; Liao, D.-F.; Tian, H.; Long, Y.-T. (2016). Discrimination of Oligonucleotides of Different Lengths with a Wild-Type Aerolysin Nanopore. *Nat. Nano, 11*, 713-718.

38. Liu, L.; Wu, H.-C., DNA-Based Nanopore Sensing. *Angew. Chem. Int. Ed.* **2016,** *55*, 15216-15222.

39.Wanunu, M.; Dadosh, T.; Ray, V.; Jin, J.; McReynolds, L.; Drndic, M.(2020). Rapid Electronic Detection of Probe-Specific Micrornas Using Thin Nanopore Sensors. *Nat. Nano,5*, 807-814.

40.Wang, Y.; Zheng, D.; Tan, Q.; Wang, M. X.; Gu, L.-Q.(2011). Nanopore-Based Detection of Circulating Micro rnas in Lung Cancer Patients. *Nat. Nano, 6*, 668-674.

41.Zhang, X.; Wang, Y.; Fricke, B. L.; Gu, L.-Q.(2014). Programming Nanopore Ion Flow for Encoded Multiplex Microrna Detection. *ACS Nano,8*, 3444-3450.

42.Zhang, J.; Yan, S.; Chang, L.; Guo, W.; Wang, Y.; Wang, Y.; Zhang, P.; Chen, H. Y.; Huang, S.(2020). Direct Microrna Sequencing Using Nanopore-Induced Phase-Shift Sequencing. *iScience,23*, 100916.

43.Shim, J.; Humphreys, G. I.; Venkatesan, B. M.; Munz, J. M.; Zou, X.; Sathe, C.; Schulten, K.; Kosari, F.; Nardulli, A. M.; Vasmatzis, G.; Bashir, R.(2013). Detection and Quantification of Methylation in DNA Using Solid-State Nanopores. *Sci. Rep,3*, 1389.

44.Laszlo, A. H.; Derrington, I. M.; Brinkerhoff, H.; Langford, K. W.; Nova, I. C.; Samson, J. M.; Bartlett, J. J.; Pavlenok, M.; Gundlach, J. H. (2013).Detection and Mapping of 5-Methylcytosine and 5-Hydroxymethylcytosine with Nanopore Mspa. *Proc. Natl. Acad. Sci. USA,110*, 18904-18909.

45.Wang, Y.; Luan, B.-Q.; Yang, Z.; Zhang, X.; Ritzo, B.; Gates, K.; Gu, L.-Q.(2014). Single Molecule Investigation of Ag+ Interactions with Single Cytosine-, Methylcytosine- and Hydroxymethylcytosine-Cytosine Mismatches in a Nanopore. *Sci. Rep,4*, 5883.

46.Zhao, Q.; de Zoysa, R. S. S.; Wang, D.; Jayawardhana, D. A.; Guan, X. (2009).Real-Time Monitoring of Peptide Cleavage Using a Nanopore Probe. *J. Am. Chem. Soc,131*, 6324-6325.

47.Wang, Y.; Montana, V.; Grubišić, V.; Stout, R. F.; Parpura, V.; Gu, L.-Q. (2015). Nanopore Sensing of Botulinum Toxin Type B by Discriminating an Enzymatically Cleaved Peptide from a Synaptic Protein Synaptobrevin 2 Derivative. *ACS Appl. Mater. Interfaces, 7*, 184-192.

48.Bell, N. A. W.; Keyser, U. F.,(2016). Digitally Encoded DNA Nanostructures for Multiplexed, Single-Molecule Protein Sensing with Nanopores. *Nat. Nano,11*, 645-651.

49.Soskine, M.; Biesemans, A.; Maglia, G.(2015). Single-Molecule Analyte Recognition with Clya Nanopores Equipped with Internal Protein Adaptors. *J. Am. Chem. Soc,137*, 5793-5797.

50.Ouldali, H.; Sarthak, K.; Ensslen, T.; Piguet, F.; Manivet, P.; Pelta, J.; Behrends, J. C.; Aksimentiev, A.; Oukhaled, A. (2020). Electrical Recognition of the Twenty Proteinogenic Amino Acids Using an Aerolysin Nanopore. *Nat Biotechnol,38*, 176-181.

51.Rodriguez-Larrea, D.; Bayley, H.(2014) Protein Co-Translocational Unfolding Depends on the Direction of Pulling. *Nat. Commun,5*, 4841.

52.Jin, Q.; Fleming, A. M.; Burrows, C. J.; White, H. S. (2012). Unzipping Kinetics of Duplex DNA Containing Oxidized Lesions in an A-Hemolysin Nanopore. *J. Am. Chem. Soc, 134*, 11006-11011.

53.Wang, Y.; Tian, K.; Hunter, L. L.; Ritzo, B.; Gu, L.-Q. (2014).Probing Molecular Pathways for DNA Orientational Trapping, Unzipping and Translocation in Nanopores by Using a Tunable Overhang Sensor. *Nanoscale,6*, 11372-11379.

54. Zhang, X.; Xu, X.; Yang, Z.; Burcke, A. J.; Gates, K. S.; Chen, S.-J.; Gu, L.-Q.(2015). Mimicking Ribosomal Unfolding of Rna Pseudoknot in a Protein Channel. *J. Am. Chem. Soc, 137*, 15742-15752.

55.Smith, A. M.; Abu-Shumays, R.; Akeson, M.; Bernick, D. L. (2015). Capture, Unfolding, and Detection of Individual Trna Molecules Using a Nanopore Device. *Front. Bioeng. Biotechnol, 3*, 91.

56.Hornblower, B.; Coombs, A.; Whitaker, R. D.; Kolomeisky, A.; Picone, S. J.; Meller, A.; Akeson, M.(2007). Single-Molecule Analysis of DNA-Protein Complexes Using Nanopores. *Nat. Meth, 4*, 315-317.

57.Celaya, G.; Perales-Calvo, J.; Muga, A.; Moro, F.; Rodriguez-Larrea, D.(2007). Label-Free, Multiplexed, Single-Molecule Analysis of Protein-DNA Complexes with Nanopores. *ACS Nano,11*, 5815-5825.

58. Zhang, X.; Xu, X.; Yang, Z.; Burcke, A. J.; Gates, K. S.; Chen, S. J.; Gu, L. Q.(2015). Mimicking Ribosomal Unfolding of Rna Pseudoknot in a Protein Channel. *J Am Chem Soc,137*, 15742-15752.

59.Zhang, X.; Zhang, D.; Zhao, C.; Tian, K.; Shi, R.; Du, X.; Burcke, A. J.; Wang, J.; Chen, S. J.; Gu, L. Q. (2017). Nanopore Electric Snapshots of an Rna Tertiary Folding Pathway. *Nat Commun,8*, 1458.

60.Niu, X.; Liu, Q.; Xu, Z.; Chen, Z.; Xu, L.; Xu, L.; Li, J.; Fang, X.(2020). Molecular Mechanisms Underlying the Extreme Mechanical Anisotropy of the Flaviviral Exoribonuclease-Resistant Rnas (Xrrnas). *Nat Commun,11*, 5496.

61.Yusko, E. C.; Bruhn, B. R.; Eggenberger, O. M.; Houghtaling, J.; Rollings, R. C.; Walsh, N. C.; Nandivada, S.; Pindrus, M.; Hall, A. R.; Sept, D.; Li, J.; Kalonia, D. S.; Mayer, M.(2017).

Real-Time Shape Approximation and Fingerprinting of Single Proteins Using a Nanopore. *Nat Nanotechnol,12*, 360-367.

62.Shasha, C.; Henley, R. Y.; Stoloff, D. H.; Rynearson, K. D.; Hermann, T.; Wanunu, M. (2014). Nanopore-Based Conformational Analysis of a Viral Rna Drug Target. *ACS Nano, 8*, 6425-6430.

63.Rotem, D.; Jayasinghe, L.; Salichou, M.; Bayley, H. (2012). Protein Detection by Nanopores Equipped with Aptamers. *J Am Chem Soc, 134*, 2781-2787.

64.Fahie, M.; Chisholm, C.; Chen, M. (2015). Resolved Single-Molecule Detection of Individual Species within a Mixture of Anti-Biotin Antibodies Using an Engineered Monomeric Nanopore. *ACS Nano* **2015,** *9*, 1089-1098.

65.Thakur, A. K.; Movileanu, L.(2018). Real-Time Measurement of Protein-Protein Interactions at Single-Molecule Resolution Using a Biological Nanopore. *Nat Biotechnol,6,1011-1020*.

66.Wloka, C.; Van Meervelt, V.; van Gelder, D.; Danda, N.; Jager, N.; Williams, C. P.; Maglia, G. (2017). Label-Free and Real-Time Detection of Protein Ubiquitination with a Biological Nanopore. *ACS Nano, 11*, 4387-4394.

67. Soskine, M.; Biesemans, A.; Maglia, G.(2015). Single-Molecule Analyte Recognition with Clya Nanopores Equipped with Internal Protein Adaptors. *J Am Chem Soc,137*, 5793-5797.

68.Galenkamp, N. S.; Soskine, M.; Hermans, J.; Wloka, C.; Maglia, G. (2018). Direct Electrical Quantification of Glucose and Asparagine from Bodily Fluids Using Nanopores. *Nat Commun, 9*, 4085.

69. Li, X., Lee, K., Chen, J., & Chen, M. (2019). A ClyA nanopore tweezer for analysis of functional states of protein-ligand interactions. *bioRxiv*, 727503.

70.Laszlo, A. H.; Derrington, I. M.; Ross, B. C.; Brinkerhoff, H.; Adey, A.; Nova, I. C.; Craig, J. M.; Langford, K. W.; Samson, J. M.; Daza, R.; Doering, K.; Shendure, J.; Gundlach, J. H.(2014). Decoding Long Nanopore Sequencing Reads of Natural DNA. *Nat Biotechnol,32*, 829-833.

71.Noakes, M. T.; Brinkerhoff, H.; Laszlo, A. H.; Derrington, I. M.; Langford, K. W.; Mount, J. W.; Bowman, J. L.; Baker, K. S.; Doering, K. M.; Tickman, B. I.; Gundlach, J. H.(2019). Increasing the Accuracy of Nanopore DNA Sequencing Using a Time-Varying Cross Membrane Voltage. *Nat Biotechnol,37*, 651-656.

72.Yan, S.; Li, X.; Zhang, P.; Wang, Y.; Chen, H. Y.; Huang, S.; Yu, H.(2019).Direct Sequencing of 2'-Deoxy-2'-Fluoroarabinonucleic Acid (Fana) Using Nanopore-Induced Phase-Shift Sequencing (Nipss). *Chem Sci,10*, 3110-3117.

73.Ledbetter, M. P.; Craig, J. M.; Karadeema, R. J.; Noakes, M. T.; Kim, H. C.; Abell, S. J.; Huang, J. R.; Anderson, B. A.; Krishnamurthy, R.; Gundlach, J. H.; Romesberg, F. E.(2020).

Nanopore Sequencing of an Expanded Genetic Alphabet Reveals High-Fidelity Replication of a Predominantly Hydrophobic Unnatural Base Pair. *J Am Chem Soc,142*, 2110-2114.

74.Derrington, I. M.; Craig, J. M.; Stava, E.; Laszlo, A. H.; Ross, B. C.; Brinkerhoff, H.; Nova, I. C.; Doering, K.; Tickman, B. I.; Ronaghi, M.; Mandell, J. G.; Gunderson, K. L.; Gundlach, J. H.(2015). Subangstrom Single-Molecule Measurements of Motor Proteins Using a Nanopore. *Nat Biotechnol, 33*, 1073-1075.

75.Cao, J.; Jia, W.; Zhang, J.; Xu, X.; Yan, S.; Wang, Y.; Zhang, P.; Chen, H. Y.; Huang, S., Giant Single Molecule Chemistry Events Observed from a Tetrachloroaurate(Iii) Embedded Mycobacterium Smegmatis Porin a Nanopore. *Nat Commun* **2019,** *10*, 5668.

76.Wendel, S. O.; Perera, A. S.; Pfromm, P. H.; Czermak, P.; Bossmann, S. H., Adaptation of Mycobacterium Smegmatis to an Industrial Scale Medium and Isolation of the Mycobacterial Porinmspa. *Open Microbiol J* **2013,** *7*, 92-98.

77.Butler, T. Z.; Pavlenok, M.; Derrington, I. M.; Niederweis, M.; Gundlach, J. H.(2008). Single-Molecule DNA Detection with an Engineered Mspa Protein Nanopore. *Proc Natl Acad Sci U S A,105*, 20647-20652.

78. Craig, J. M.; Laszlo, A. H.; Brinkerhoff, H.; Derrington, I. M.; Noakes, M. T.; Nova, I. C.; Tickman, B. I.; Doering, K.; de Leeuw, N. F.; Gundlach, J. H.(2017). Revealing Dynamics of Helicase Translocation on Single-Stranded DNA Using High-Resolution Nanopore Tweezers. *Proc Natl Acad Sci U S A, 114*, 11932-11937.

79. Sztuba-Solinska, J.; Shenoy, S. R.; Gareiss, P.; Krumpe, L. R.; Le Grice, S. F.; O'Keefe, B. R.; Schneekloth, J. S., Jr.(2014). Identification of Biologically Active, Hiv Tar Rna-Binding Small Molecules Using Small Molecule Microarrays. *Journal of the American Chemical Society,136*, 8402-8410.

80.Kelly, J. A.; Olson, A. N.; Neupane, K.; Munshi, S.; San Emeterio, J.; Pollack, L.; Woodside, M. T.; Dinman, J. D.(20202). Structural and Functional Conservation of the Programmed -1 Ribosomal Frameshift Signal of Sars Coronavirus 2 (Sars-Cov-2). *J Biol Chem, 295*, 10741-10748.

81.Velagapudi, S. P.; Cameron, M. D.; Haga, C. L.; Rosenberg, L. H.; Lafitte, M.; Duckett, D. R.; Phinney, D. G.; Disney, M. D.(2016). Design of a Small Molecule against an Oncogenic Noncoding Rna. *Proceedings of the National Academy of Sciences of the United States of America, 113*, 5898-5903.

82.Rzuczek, S. G.; Colgan, L. A.; Nakai, Y.; Cameron, M. D.; Furling, D.; Yasuda, R.(2017). Disney, M. D., Precise Small-Molecule Recognition of a Toxic Cug Rna Repeat Expansion. *Nature chemical biology,13*, 188-193.

83.Schibel, A. E.; An, N.; Jin, Q.; Fleming, A. M.; Burrows, C. J.; White, H. S.(2010). Nanopore Detection of 8-Oxo-7,8-Dihydro-2'-Deoxyguanosine in Immobilized Single-Stranded DNA Via Adduct Formation to the DNA Damage Site. *J Am Chem Soc* **2010,** *132*, 17992-17995.

Chapter Four

Maximizing Sensitivity of Dopamine Detection

4.1 Introduction

The brain activity mapping (BAM) project proposes to measure every action potential from every neuron (Alivisatos et al., 2012). Since neurotransmitters play a central role in the generation and propagation of action potentials, the goal of developing tools to not only detect but also to quantify neurotransmitters dovetails neatly into the BAM ideals. Tools capable of providing temporal profiles of neurotransmitters at the single molecule level will ultimately be of great utility. There are a couple of reasons for this. Firstly, deficiency of or excessive production of neurotransmitters is associated with brain pathologies such as Parkinson's disease and Huntington's disease. These pathologies constitute a gargantuan public health challenge. Secondly, because of the critical role that neurotransmitters play in brain pathology neurotransmitter receptors as well as neuropeptides and proteins have emerged as important targets for therapeutic drugs development (Narahashi, 2000). Additionally, substances such as cocaine, opiates, nicotine, ethyl alcohol and several other recreational drugs are capable of mimicking or even interfering with actions of neurotransmitters thereby exerting potent effects on human behavior (Hyman, 2005).

Dopamine is an important neurotransmitter that has gained much attention because of its implication in substance abuse. Measurement of dopamine at the single-molecule level remains a challenge mainly due to its low basal physiological concentrations (Fang et al., 2013). Chapter three presented a novel nano-sensing platform that is capable of real time monitoring dopamine in the presence of other neurotransmitters. However, it was noted that a major drawback of the

platform was that it could not detect dopamine at low concentrations. This chapter presents efforts to address this drawback and enhance sensitivity.

A myriad of factors combines to influence how an aptamer behaves in and interacts with a biological pore. To begin with, the aptamer must move from the bulk solution and enter the pore through electro-diffusion. To do so it must overcome the free energy barrier at the pore entrance (Martin et al., 2009; Movileanu et al., 2005; Sung & Park, 1996). Once in the pore the aptamer is submerged in an ionic space where its behavior is influenced by interionic interactions. Interionic effects come into play when ions are submerged in an ionic space with a net charge opposite to that of the ion (Falkenhagen, 1931; Fologea et al., 2005). In this specific case, the negatively charged aptamer is submerged in an electrolyte solution inside a positively charged pore vestibule and constriction zone. The aptamer can be captured in the pore or translocate immediately.

In nanopore sensing, the capture site for an aptamer is created inside the pore by site-directed mutagenesis or targeted chemical modification (Bayley & Cremer, 2001).The charge distribution inside the lumen of the pore determines the ion selectivity of the pore as well as the capture rate and dwell time (Maglia et al., 2008). The motion of the aptamer inside the pore is driven by voltage, typically a few hundred millivolts, applied between two electrodes placed in the chambers. DNA capture by nanopores is notoriously inefficient and only occurs above a threshold potential (Henrickson et al., 2000; Maglia et al., 2008). It has been reported that at voltages close to the threshold, 1 DNA molecule in every 1,000 that collides with the pore is translocated and the rest are captured (Meller, 2003). Aptamers have relatively low molecular weight, and their capture rate is dominated by the barrier at the entrance to the pore. As the electric field increases, the height of the barrier decreases. Consequently, the capture rate

increases exponentially with the voltage gradient (and molecular weight)(Grosberg & Rabin, 2010). It is desirable to establish *an optimum voltage* for each pore, aptamer, and electrolyte combination. However, bilayers are susceptible to breaking at high voltages. Hence it is important to establish the most efficient and practicable operating voltage.

Besides voltage there are other factors that contribute to the capture of analytes in pores. Some of these are the type of ions in the buffer (de Zoysa et al., 2009; Fologea et al., 2005; Yan et al., 2019), ionic concentration (Bello et al., 2019; Vu et al., 2019), pH of buffer and temperature (L. Yeh et al., 2012; Zhang et al., 2013). It has been demonstrated that an electrolyte solution containing monovalent counterions can alter the electrophoretic mobility of DNA, and by extension DNA dwell time in a nanopore, in different ways. These include: changing bulk properties of water (Marcus, 1997), modifying DNA conformation, and affecting the preferential binding of counter-ions to DNA (Hud & Plavec, 2003; McConnell & Beveridge, 2000; McFail-Isom et al., 1999; E. Stellwagen et al., 2005; N. C. Stellwagen et al., 1997). The dwell time is inversely proportional to DNA translocation velocity, directly proportional to the valence of the ion and inversely proportional to the radius. Counter-ions affect the mobility of DNA by altering the condensed counter-ion cloud surrounding the DNA molecules and by binding in the minor groove of DNAs (charge screening) (De Marky & Manning, 1975, 1976; Manning, 1978). The binding lasts 10 times longer for divalent ions than monovalent ions (Korolev et al., 1999; Yoo & Aksimentiev, 2012). The condensed counter-ion cloud is in constant flux. Divalent ions also cause greater conformational change, and offer more charge screening (Cheng et al., 2006; Dong et al., 2009; Guéroult et al., 2012; Heddi et al., 2007; Subirana & Soler-Lopez, 2003). To a large extent both DNA conformation and DNA mobility are very sensitive to the cation environment.

When an ion is immersed in an ionic space (in this case buffer) containing ions with a net charge opposite to its own, interionic forces exert a drag force on the ion which slows down its mobility in an electric field. DNA being negatively charged is slowed down by cations. All atom molecular dynamics simulations have demonstrated that the number of cations bound in the groove increases with increasing electrolyte concentration. Furthermore, the smaller the ion the stronger the covalent bond formed in the DNA grooves, and the longer the bond lasts (Vu et al., 2019). Additionally, the affinity of DNA for cations is determined by the cation type and valence. Previous studies showed that the binding affinities of monovalent cations to DNA are inversely proportional to the radius of the specific binding ion. For example, DNA affinity decreases in the order Ca > Mg ≫Li> Na ≈ K (Korolev et al., 1999). DNA does not exhibit selectivity for Na^+ or K^+ in water solutions either in the absence or in the presence of Ca^{2+} and/or Mg^{2+} (Korolev et al., 1999). The ionic radii and viscosity coefficients of the cations are as follows*:* Mg^{2+}(0.065 nm;0.385); Ca^{2+}(0.1 nm;0.298); Li+(0.069 nm;0.146); Na+(0.102 nm;0.085) and K+(0.138 nm;0.085). The divalent ions have higher viscosity coefficients and are therefore expected to slow down the translocation velocity more. More specifically, the binding of counter-ions partially neutralizes the negatively charged phosphate backbone; which in turn decreases the overall effective net charge and mobility of the DNA molecule (Dong et al., 2009; Hud & Plavec, 2003; E. Stellwagen et al., 2005). Most research on nano-sensing has employed 1M KCl buffer. However, it was reported that LiCl increased the dwell time of DNA in solid state nanopores and in the alpha hemolysin nanopore (Bello et al., 2019; Vu et al., 2019). In both pores the increase in dwell time was even more pronounced if a concentration gradient was explored. There is a lacuna in extant literature in the use of LiCl and divalent ions with the MspA pore.

The aim of the experiments presented in this chapter was to enhance sensitivity of dopamine detection and quantification by manipulating the charge distribution in the pore lumen, employing different ion types at different concentrations, altering bias voltage, and employing salt concentration gradients. The rest of the chapter is organized as follows:

In the Material and Methods section, details of the experimental procedures and the data analysis approach are reported.

In the Results and Discussion section, the data on mutant pore comparisons, ion species comparisons, ionic concentrations experiments, asymmetric ionic concentrations experiments, and voltage experiments are presented. Additionally, the implications and the limitations of the data and findings are discussed.

The significance section articulates the implications of the study. This is followed by the conclusion section where some conclusions are drawn based on the findings.

4.2 Materials and Methods

The materials and methods were described in detail in chapter two. Additional information, if any, pertaining to each set of experiments is given in the specific set of experiments.

4.3 Results and Discussion

4.3. 1 Mutation effects on aptamer residence time

In the first set of measurements the residence time, the ON time and the dopamine binding time were characterized for the two aptamers M2 and M7. Multiple experiments were conducted with each pore on different days. To control for external factors such as noise and room temperature, a completely randomized design was adopted. In this design subjects are randomly assigned to treatments (Ledolter & Kardon, 2020). In the present case the order in

which M2 and M7 experiments were conducted on a particular day was completely randomized. The residence time was measured as the time from the start to the end of blockade events. The data from the different experiments was first analyzed individually before being aggregated into a single data set. Data analysis was three-fold. The first step in analysis involved exploring patterns in the data by generating histograms and fitting curves. Fig 4.1 below is a depiction of the histograms generated using different bin sizes.

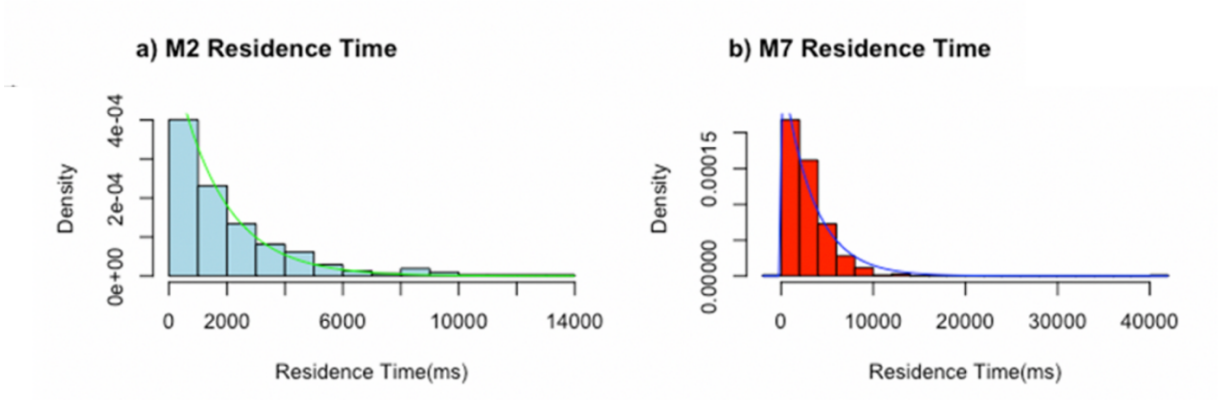

Fig 4. 1 : Data exploration and curve fitting.

Data from both pores was closely approximated by exponential functions.

The statistical approaches chosen were informed by the distribution of the residence times which was exponential in nature. Three approaches were employed. Namely these are bootstrapping, Mann Whitney U test and prosaic student t-test. The bootstrap method employs a resampling approach to estimate sampling distributions. It takes the sample data that a study obtains, and then resamples it with replacement over and over to create many simulated samples (Gareth James, 2013; Thomas J. DiCiccio & Bradley Efron, 1996). For example, a sample of 1000 events can be selected independently and with replacement, from a data set with 5000 events, and the process can be repeated 100 times. This is the equivalence of conducting 100 experiments generating 100000 events. Each of these simulated samples possesses its own

properties, such as the mean and standard deviation. These simulated samples are used as the foundation for confidence intervals and hypothesis testing in a process that is akin to conducting multiple experiments. Bootstrapping is not encumbered by the assumptions associated with underlying distributions (Gareth James, 2013; Thomas J. DiCiccio & Bradley Efron, 1996). It is, therefore often used as an alternative to statistical inference based on the assumption of a parametric model when that assumption is in doubt, or where parametric inference is impossible or requires complicated formulas for the calculation of standard errors. Apart from a being straightforward way to derive estimates of standard errors and confidence intervals for complex estimators of the distribution, such as percentile points, proportions, odds ratio, and correlation coefficients, bootstrap is also a robust way to control and check the stability of the results. It's simplicity and cost effectiveness confer advantages to it over other methods.

Bootstrapping was performed using r-software to establish the means and standard deviations and the confidence intervals. Bootstrap was the preferred analytical approach because it does not assume that the data is normally distributed. To add extra robustness and check for consistency the data for the residence times was also subjected to traditional inferential statistics testing methods. Since many experiments were conducted, means were computed for each experiment and recorded. The Mann Whitney U tests were performed to examine if there were statistical differences on the mean and the median.

The Mann-Whitney U test (H. B. Mann & D. R. Whitney, 1947) is a non-parametric test that can be used as an alternative to the unpaired t-test. It is used to test the null hypothesis that two samples come from the same population, have the same median or, more precisely, whether observations in one sample tend to be larger than observations in the other. Although it is a non-parametric test it does assume that the two distributions are similar in shape. It has great utility

when the underlying distribution is not normal or is not known. It ranks all the observations in the groups from the smallest to the largest regardless of which group they come from. The ranks for each group are then summed and the outcomes are compared. When large samples are involved as in this case the ranks assume a normal distribution and the t test for independent samples yields the same results as the Mann Whitney test. A p value of <0.05 indicates that variables being compared are statistically significantly different at the 0.05 level of statistical significance.

The summary of the analyses for the comparison between M2 and M7 pores is presented in Fig 4.2, Fig 4.3, and Fig 4.4 below. The histograms for the residence times are presented in Fig 4.2. The most prominent features of these plots are:

(i) The mean residence time for M7 (mean=2.9s ± 0.9s) was higher than that of M2 (mean=2.2±0.3s). This was statistically significantly different at the 0.05 level of significance using the Mann Whitney test. The bootstrap confidence intervals for the means were (1.96s; 2.36s) and (2.58s; 3.28s) for M2 and M7 respectively. The median values for M2 and M7 were 1.9s and 2.3s respectively. Three things are noteworthy. Firstly, the confidence intervals of the means medians do not overlap confirming the earlier finding that the two means were statistically significantly different. Secondly, the calculated means and standard deviations all fall in the confidence intervals calculated by bootstrapping. Thirdly, the huge standard deviations illustrate that there is a considerable spread in event characteristics. This is in keeping with prior findings (Kowalczyk et al., 2012a; Van den Hout et al., 2010). This was attributed to interactions between the DNA and pore walls which are particularly prominent in pores under 5 nm in diameter (Wanunu et al., 2008; I.-C. Yeh & Hummer, 2004). However, it is noteworthy

that the prior studies were conducted in solid state nanopores with larger pore diameters. The concordance between the results from bootstrap method and the traditional t-test approach again lends credibility to the data and analysis. Further evidence was obtained by computing the Mann Whitney U test which yielded a p value of <0.0001.

(ii) An examination of the residence times revealed that only 11% of the M2 events lasted longer than 4000ms. In comparison 23% of the M7 events lasted more than 4000ms. Proportionally, there are more M7 events with longer dwell times.

(iii) There was a strong correlation (p=0.74) between residence time and dopamine binding. A priori this was not surprising as it is intuitive that the longer the aptamer is anchored in the pore the more likely that dopamine will bind.

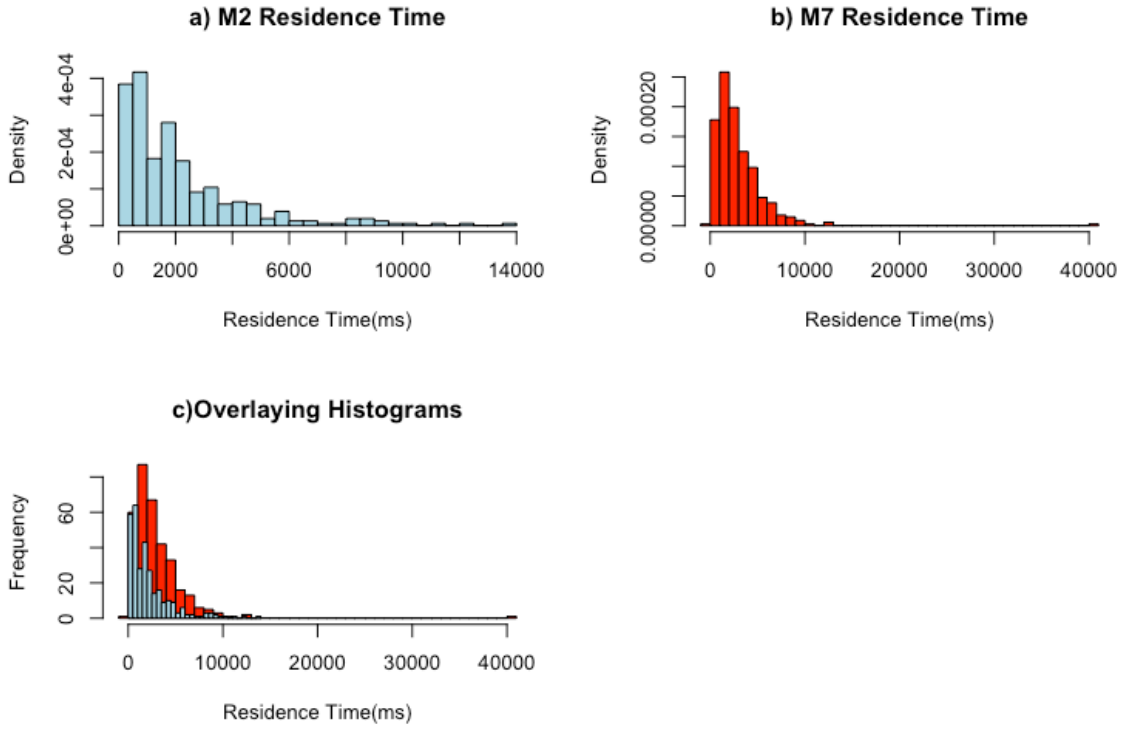

Fig 4. 2: Comparison of the residence times for the M2 and M7 pores.

a) 11% of the M2 pore events were longer than 4000ms. There were a few outliers beyond 6000ms b) 23% of the events recorded with the M7 pore were for a duration longer than 4000ms. c) An overlay of the histograms demonstrates that the peaks fall in the same bin.

The differences can be attributed to the interactions between the aptamer and the charges in the pore. The importance of interactions between the pore and analytes was previously underscored by (Bezrukov et al., 1996; Bezrukov & Kasianowicz, 1997; Lubensky & Nelson, 1999; Martin et al., 2009; Meller, 2003).

A summary of the results of the analysis of the ON Time data is presented in Fig 4.3. The mean on times were 188.7ms and 314.8ms for M2 and M7 respectively. The frequency (F) was calculated using the equation $F=1/T_{on.}$ The respective values were 0.005 events-ms^{-1} and 0.003 events-ms^{-1}. Additionally, "bootstrapping" was performed on the mean ON Time of the two pores. The confidence intervals for the pores were (177.5; 200.7) and (296.2; 333.2) for M2 and M7 respectively. It is noteworthy that the confidence intervals of the means do not overlap. This confirms that the ON times of the two pores are statistically significantly different. M7 has the higher ON Time. Conversely M2 has a higher frequency of events. This is to be expected as the residence time for M2 is shorter than that of M7. Hence M2 has more events but of a much shorter duration. The finding that the two pores have different frequencies is in keeping with other studies. Specifically (Bezrukov & Kasianowicz, 1997) reported that the charge state of a channel impacts the frequency with which polymers enter into its pore.

Fig 4.4 presents a summary of the analysis of the dopamine binding times. The dopamine binding time corresponds to the OFF time. The means were 254.4ms for M2 and 246.7ms for M7. The confidence intervals of the bootstrapped means were (239.6ms; 269.3m s) and (236.7ms; 255ms). The overlap in the confidence intervals reveals that the two are not statistically different at the 0.05 level of significance. The data were pooled together, and independent samples

t tests were performed. The analysis concluded that the difference was not statistically significant at the 0.05 level of significance. Taken together data from this group of experiments demonstrated statistically significant increases in the aptamer residence time and the ON Time. However, these increases did not translate to a statistically significant increase in dopamine binding time.

These experiments demonstrated that altering the charge distribution in the pore has the potential to alter residence time of the aptamer in the pore. Experiments done in chapter three demonstrated that different rings of charges have different effects on aptamer capture. Previously it was also reported that negative charges at the constriction of the wild type MspA pore prohibited DNA translocation (Butler et al., 2008; Derrington et al., 2010, 2011). The M2-pore used in the current experiments was created by replacing all the negative charges in the constriction with neutral charges. These mutants were created with the aim of facilitating DNA translocation. The current study seeks to create a balance between facilitating translocation and slowing down translocation to allow dopamine binding and detection. To optimize sensitivity a balance must be struck between facilitating translocation and slowing down translocation to allow dopamine binding and detection.

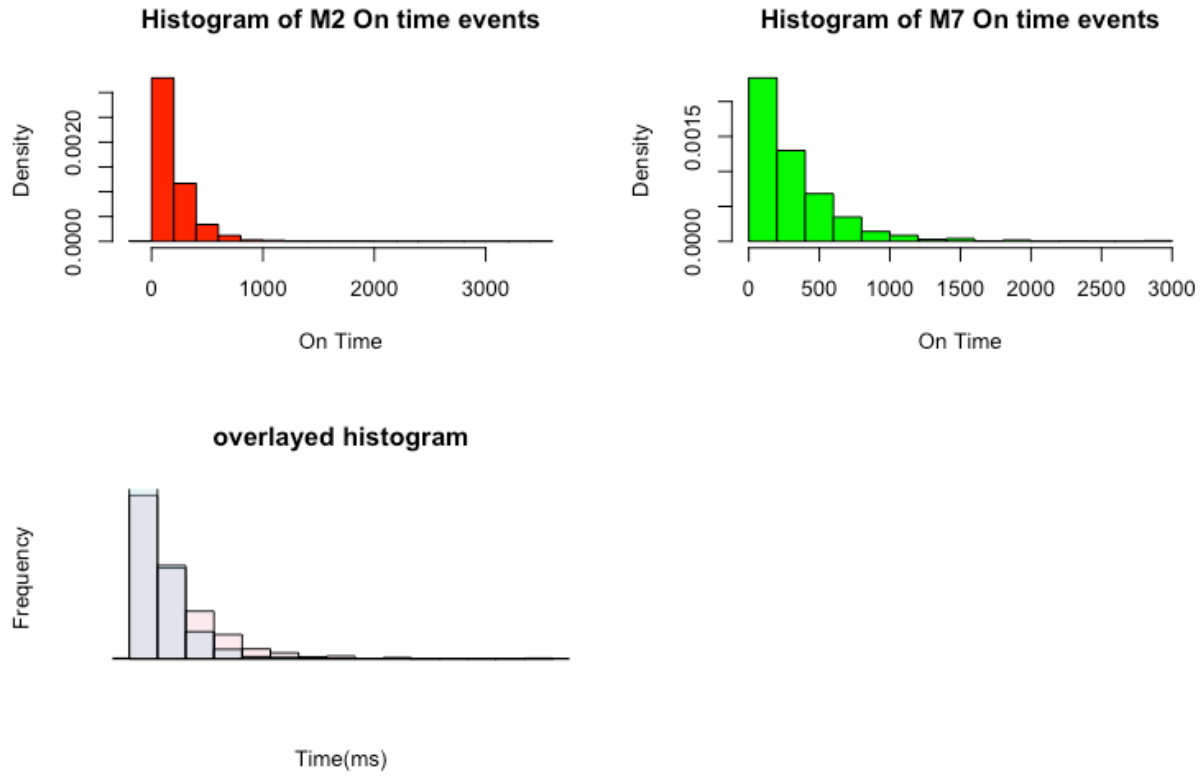

Fig 4. 3: On Time analysis.

The overlay shows that generally there were more events with longer dopamine binding time with the M2. However, the differences were not statistically significant.

4.3.2 Effect of bias voltage on Residence time, binding time and on time

To examine the effect of bias voltage several experiments (n=6) were conducted with 1M KCl buffer, 50uM dopamine and 10uM aptamer. At voltages below 100mV, insertion of the aptamer into the pore was noted but resolvable events were very infrequent. Consequently, a decision was made to explore the voltage dependency at higher voltages. The experiments were done at 100 mV,120mV, 150mV and 180mV and at room temperature. In each case the electrode in the cis side was grounded. Each experiment was run for at least 15 minutes, and data was acquired at each of the voltages for 3 minutes. Thus, in each set of experiments the voltage was set at the different levels for the same amount of time. To control for possible variations in

external factors, the order in which the voltages were set was assigned by complete randomization. Data was collected on residence time, dopamine binding time and on time. All the experiments were conducted with the M2 mutant. The mean, standard deviation and standard error of the mean were computed. Data analysis took the form of one-way Anova and bootstrapping. All statistical tests were conducted at the 0.05 level of significance. A summary of the findings is presented in Fig 4.4 below.

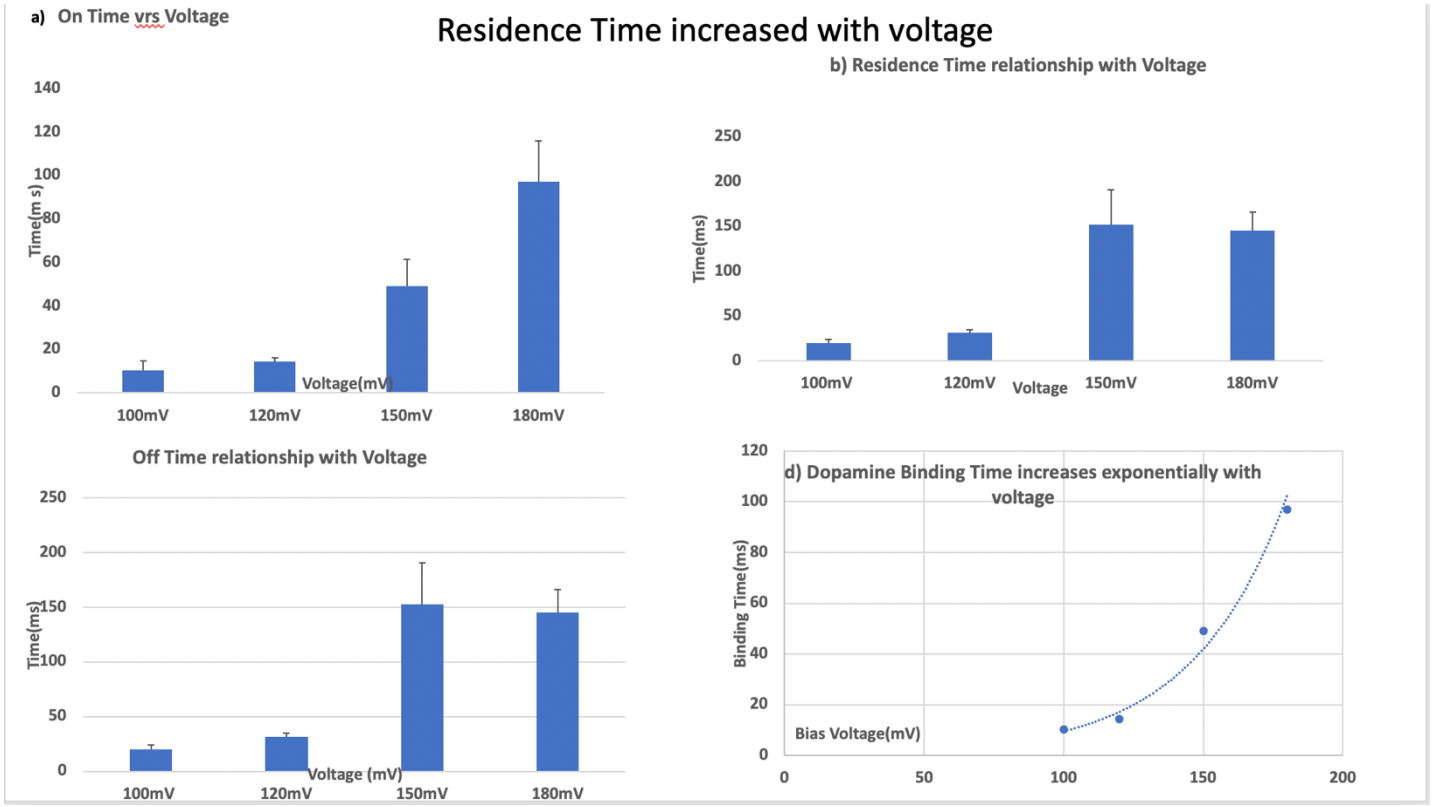

Fig 4. 4: **Dependence of different times on voltage.**

a) Dopamine binding time increased with voltage from100mV to 180mV. The differences were statistically significant. b) Residence time increased with voltage from 100mV to 150mV and then decreased. The increases were statistically significant but the decreased noted between 150mV and 180mV was not significant. c) ON time increased with voltage but there was no statistically significant difference between the times at 180mV and 150mV. d) The increase in the dopamine binding time was exponential in shape.

There were few important observations from the data. These are:

(i) All the resident times increased with voltage. The differences between the lower voltages (100mV and 120mV) on one hand and the higher voltages (150mV and 180mV) were very pronounced and statistically significant.

ii) A potential of 180 mV produced the longest binding time which was statistically significantly different from times recorded with the other voltages. Additionally, the ON Time for 180mV is lower than that at 150mV. Conversely, the frequency of events at 180mV is higher. This is in sync with previous findings that the frequency of events increased exponentially with increase in voltage(Wanunu et al., 2010a).

(iii) There is a small increase from 100mV 120mV and a big jump from 120mV to 150mV. This is true for all three parameters.

iv) At the low voltages (not depicted on Fig 4.5) the number of events were insignificant suggesting that the aptamer rarely entered the pore. This is in keeping with the theory that for polymers to insert into a pore a free energy barrier needs to be overcome first (Bezrukov et al., 1996; Kasianowicz et al., 1996). This barrier is bigger for nanosized pores such as the MspA pore. A higher threshold voltage is therefore required to propel the aptamer into the pore (Storm et al., 2005; Van Dorp et al., 2009). Furthermore, (Wanunu et al., 2010a) reported that the capture rate increased exponentially with voltage increases.

The finding that residence time increased with voltage is at variance with previously reported values for solid state nanopores (Lubensky & Nelson, 1999; Meller et al., 2000,

2001) and for the alpha-hemolysin (Kasianowicz et al., 1996; Lubensky & Nelson, 1999; Meller, 2003) protein pores showing an inverse relationship between translocation time and applied voltage. However, they are in agreement with results obtained for smaller diameter pores (Heng et al., 2004). There are some important differences between the current study and those reported in the literature. Firstly, some of the reports that observed an inverse relationship were conducted with solid state pores and with DNA strands that were longer than 100 nucleotides. The current study employed a much shorter aptamer in a protein pore. Secondly, all the studies used pores with bigger diameters (>6nm) in contrast with the ~1nm diameter of the MspA pore used in the current study. Thirdly, although the alpha-hemolysin studies used a protein the pore is wider than the MspA and the studies also employed longer DNA chains. Fourthly, the study that reported findings like the current study employed solid state nanopores whose diameters are similar in size to the MspA pore. However, that study used voltages between 200mV and 500mV.

Extant literature review reveals some gaps. The studies on residence times were based on proteins translocating through nanopores. There were no studies on aptamers anchored in biological pores. (Wanunu et al., 2008, 2010b) observed an exponential voltage dependence on translocation times. Additionally, the translocation times scaled differently for DNAs of different lengths. For short DNA molecules, in the range 150–3500 bp, the variation could be described by an exponent of 1.40, whereas for longer molecules, an exponent of 2.28 dominated. The current study finds an exponential relationship howbeit for a short aptamer 20bp, and the residence time rises with the voltage rather than decrease. The current study employed voltages between 100mV and 180mV. Extrapolations cannot be made to cover voltages outside this range.

4.3.3 Effect of Ionic Concentration and Ion Type on Binding Time and Aptamer Residence Time.

In chapter three it was noted that at low concentrations of KCl, neither aptamer insertion in the pore nor dopamine binding was noted. However, dopamine binding and aptamer insertion were noted when 1M KCl electrolyte was used. This suggested that either dopamine binding or aptamer capture in the pore or both were dependent on the concentration of the buffer. To examine this several experiments (n=3 at each concentration with each ion type) were conducted at 300mM, 600mM and 1M. Additionally the dependence of aptamer capture and dopamine binding on ion type was also examined. The ions used in this study were KCl, NaCl and LiCl. KCl and NaCl experiments were done at 180 mV whereas 20mV was used for LiCl. These ions were selected because they are all monovalent, and therefore a priori are expected to exhibit similar behavior. As with previous experiments the order in which the experiments were carried out was completely randomized. The results are presented in Fig 4.7 below.

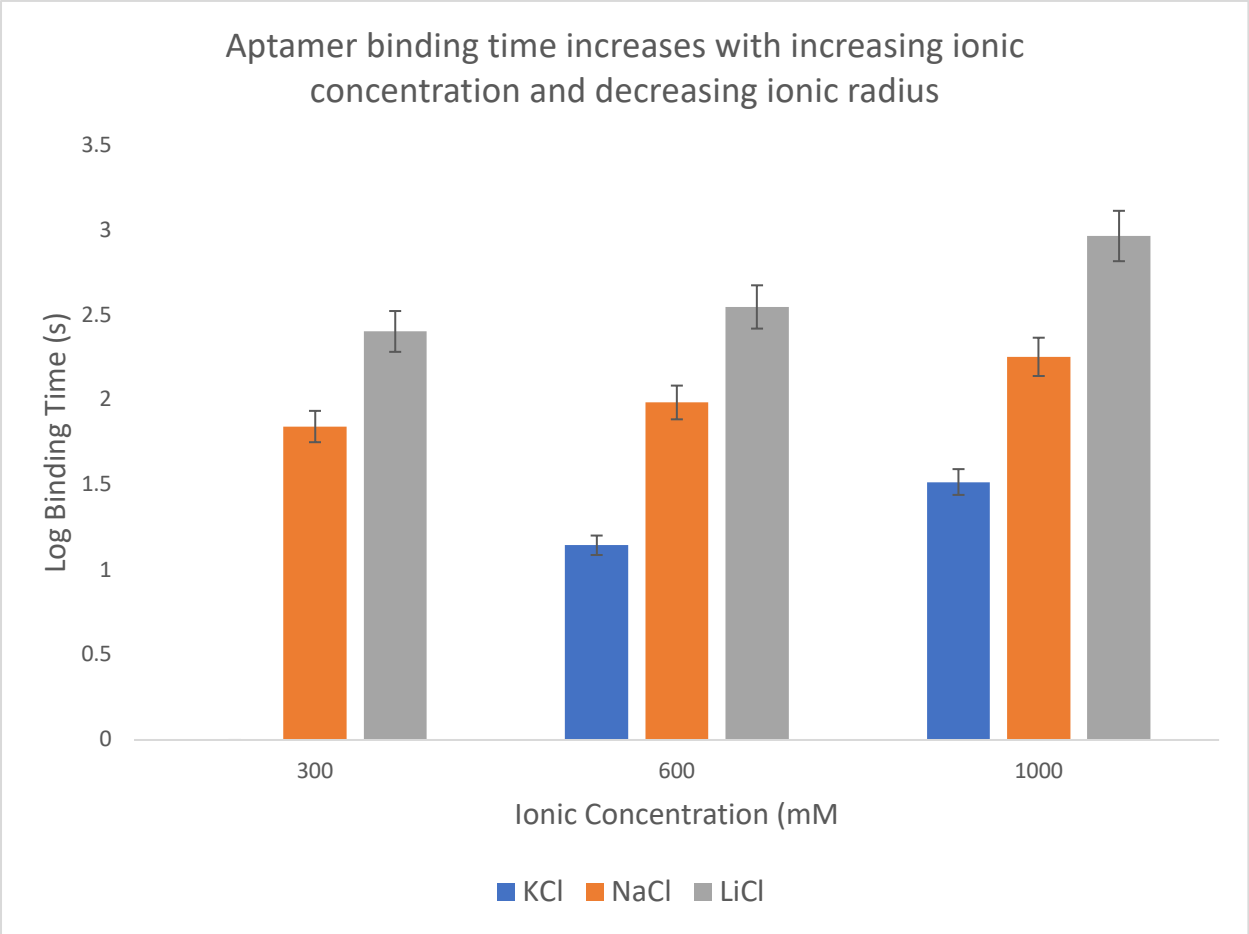

Fig 4. Dopamine binding time and aptamer residence time increase with ionic concentration for all ions

Dopamine binding time increases with ionic concentration in the order LiCl>>NaCl>KCl. The binding time is inversely proportional to the ionic radius The KCl and NaCl were conducted with the bias voltage set at 180mV, while the LiCl experiments were at 20mV.

A few salient observations can be made.

(i) Both dopamine binding time and aptamer residence time increased with an increase in salt concentration. For a given concentration, the number of events was found to scale inversely with the translocation time.

(ii) Although the three ions were all monovalent, they affected dopamine binding differently. Specifically, both dopamine binding and aptamer residence time at any given concentration were

inversely proportional to the size of the ion. LiCl with the smallest ionic radius demonstrated the most significant change.

(iii) The amplitude of the current blockage and the percentage change in conductance with block increased with an increase in concentration as shown in Fig 4.6 below from a representative trace of NaCl.

As was noted earlier no events were detected with 300mM KCl. There are a few possible explanations for this. Firstly, it is possible that there are events of such a small amplitude and short duration that the instrument is not able to resolve them. Secondly, it is possible that the aptamer was not inserted into the pore at all. If it had been inserted in the pore, some current modulation due to the presence of the aptamer would have been recorded. Third, in measuring the salt dependence of ion transport and DNA translocation through solid state nanopores in the concentration range 0.1mM to 1M(Smeets et al., 2006) demonstrated the existence of a cross-over point at which DNA translocation causes no current blockage. In KCl this cross-over point was found to be between 330mM and 410mM. They also noted that at concentrations below the cross-over point instead of DNA translocation causing current reduction it resulted in spike-like current increases They argued that the cross over point occurs when the current flow due to flow of charge carrying DNA offsets the current decrease due to the DNA occupying the pore.

In these experiments we demonstrated as depicted in Fig 4.5 above that changing the buffer from 1M KCl which is typically used in nanopore experiments to 1M LiCl yielded a 1.72-fold increase in the residence time and a 3.65-fold increase in dopamine binding time. Such an increase is not only beneficial in this study but can also be translated into gains in read out resolution in nanopore measurements in general. Fig 4.6 presents representative traces depicting

the dramatic increase blocked current and residence time that makes it much easier to resolve the signature pattern that accompanies dopamine binding.

Although using LiCl and NaCl managed to demonstrate dopamine binding at low concentration the resolution was poor. This set of experiments demonstrated that better sensitivity can be achieved by using different ion types and using higher concentrations. (Kowalczyk et al., 2012a) achieved a 5-fold increase in DNA translocation time by replacing 1M KCl with 1M LiCl. The ion type effect demonstrated here is consistent with findings that different ions impact the electrophoretic mobility of DNA differently(E. Stellwagen et al., 2005). Using molecular dynamics simulations (Kowalczyk et al., 2012a) elucidated that the difference between the impact of the ion type stems from both ion size and ion type. It was shown that transient binding of counter ions partially neutralizes the DNA charge. Moreover, the smaller ions tend to form stronger bounds that last longer compared to the larger ions. As the concentration increases the number of ions bound to the DNA also increases thereby slowing down its translocation.

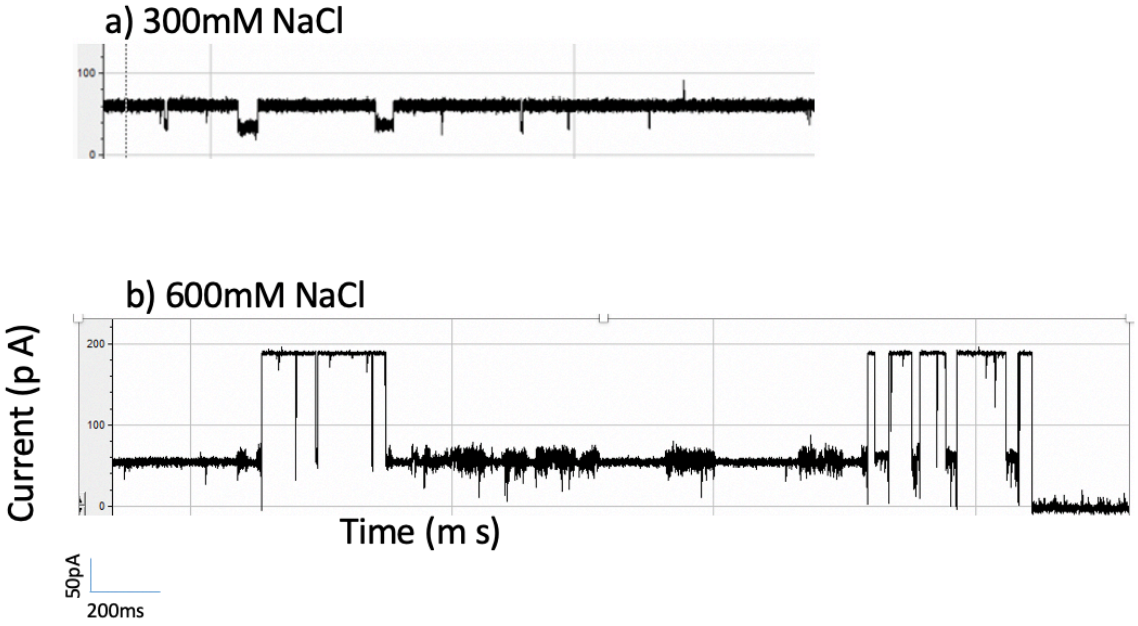

Fig 4. 5: Increase in concentration of the ions resulted in better read out resolution.

a) Representative trace from 300mM NaCl showing smaller and shorter but more events. b) Doubling the concentration yielded larger current blockages with longer duration. This trend was true for all ions but was most pronounced with LiCl.

The divalent ions, Mg^{2+} and Ca^{2+} have a higher affinity for DNA than the monovalent ions(Bai et al., 2007). The higher affinity of divalent cations stems from the stronger Coulombic interactions between divalent cations and the DNA (Owczarzy et al., 2008). Consequently, fewer divalent cations are required to neutralize the DNA charge compared to monovalent ions(Dove & Davidson, 1962). The implication for the current study is two-fold. Firstly, a lower concentration of divalent ions produces more DNA charge neutralization resulting in longer DNA translocation duration. Secondly, if both divalent ions and monovalent ions are present in the buffer, there is a preference for divalent ion binding. Taken together these implications informed the hypothesis that divalent ions demonstrate better sensitivity for detection of dopamine binding in low concentrations in protein pores. This hypothesis was tested by the next series of experiments. Previous attempts to employ divalent ions failed because in the presence of divalent ions the DNA adhered to the membrane (Kowalczyk et al., 2012a). However, the experiments were conducted with solid state nanopores. This finding is hardly surprising given that Mg^{2+} are the preferred ion for adhering DNA to inorganic surfaces such as mica and SiO_2 (Kowalczyk et al., 2012b).

4.3.4 Employing $MgCl_2$ to enhance detection of dopamine.

This series of experiments had three sets of experiments. First, a control study was conducted whose aim was to establish if aptamer insertion could be detected in 200mM $MgCl_2$.An additional aim was to establish a signature pattern of the current blockage in $MgCl_2$ buffer. Fig

4.9a) shows that both aims were successfully accomplished. The mean dopamine binding time in 200mM $MgCl_2$ was 115.9± 80.2ms. This was much higher than the 0 recorded with 200mM KCl but much lower than the 2.9s obtained using 1M KCl, Additionally, the mean current blockage measured as a ratio of the blocked current to open pore current was 59.9±10.3%. These experiments demonstrated that $MgCl_2$ could be used as buffer in the detection of dopamine binding. Moreover, by adding 10mM $MgCl_2$ to 300mM KCL we demonstrated that dopamine binding could now be detected at a concentration which had previously been problematic.

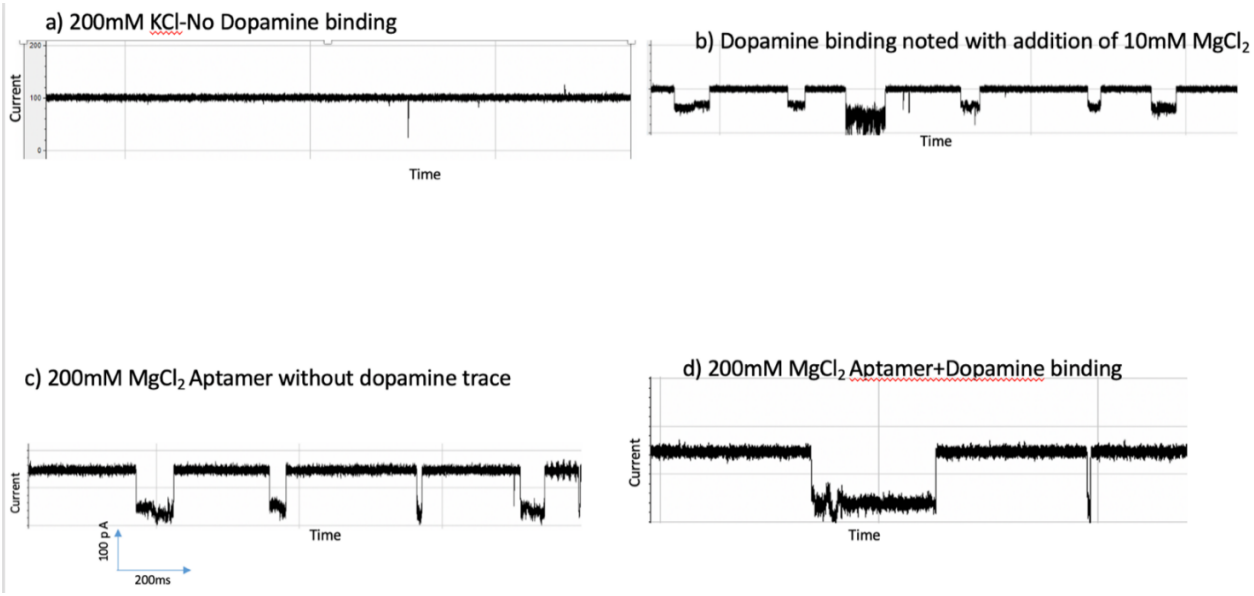

Fig 4. 6:Dopamine detection in the presence of $MgCl_2$.

a) No aptamer insertion detected in 200mM KCl. b) Soon after addition of 10mM $MgCl_2$ several dopamine binding events were detected. c) In 200mM $MgCl_2$ aptamer insertion in pore was easily detected. d) When dopamine was added on the trans side signature current blockage associated with dopamine binding were detected.

4.3.5 Dopamine detection in physiological concentrations

Having demonstrated that divalent ions have the potential to enhance dopamine measurement in low concentrations as a proof of concept, attention was directed towards detecting dopamine in physiological conditions. To achieve this artificial cerebrospinal fluid (ACSF) was used as the buffer. The concentration of KCl in ACSF was 140mM. The solution on the trans side contained 50μM dopamine. The experiment was carried out in four stages. Firstly, the experiment was conducted with an aptamer only in the cis side to obtain a baseline reference trace. Secondly, dopamine was added to the trans side to establish a signature current pattern for dopamine in ACSF. In the third stage the experiments of the first stage were repeated, but this time 10mM $MgCl_2$ was added to the cis after 3 minutes. The purpose of the third set of experiments was to establish the pattern produced when the aptamer is in the pore in the absence of dopamine. Finally, the last set of experiments was a repeat of the second set of experiments with 10mM $MgCl_2$ was added to the electrolyte on the cis side after 3 minutes.

As expected, the traces in the absence of $MgCl_2$ depicted no evidence of aptamer capture in the pore. However, upon the introduction of 10mM $MgCl_2$ multiple events were recorded. The events have a very small current blockage amplitude and were of a short duration. It was not possible to visually decipher the two conformational state signature that is characteristic of dopamine binding. Fig 4.8 below presents representative traces.

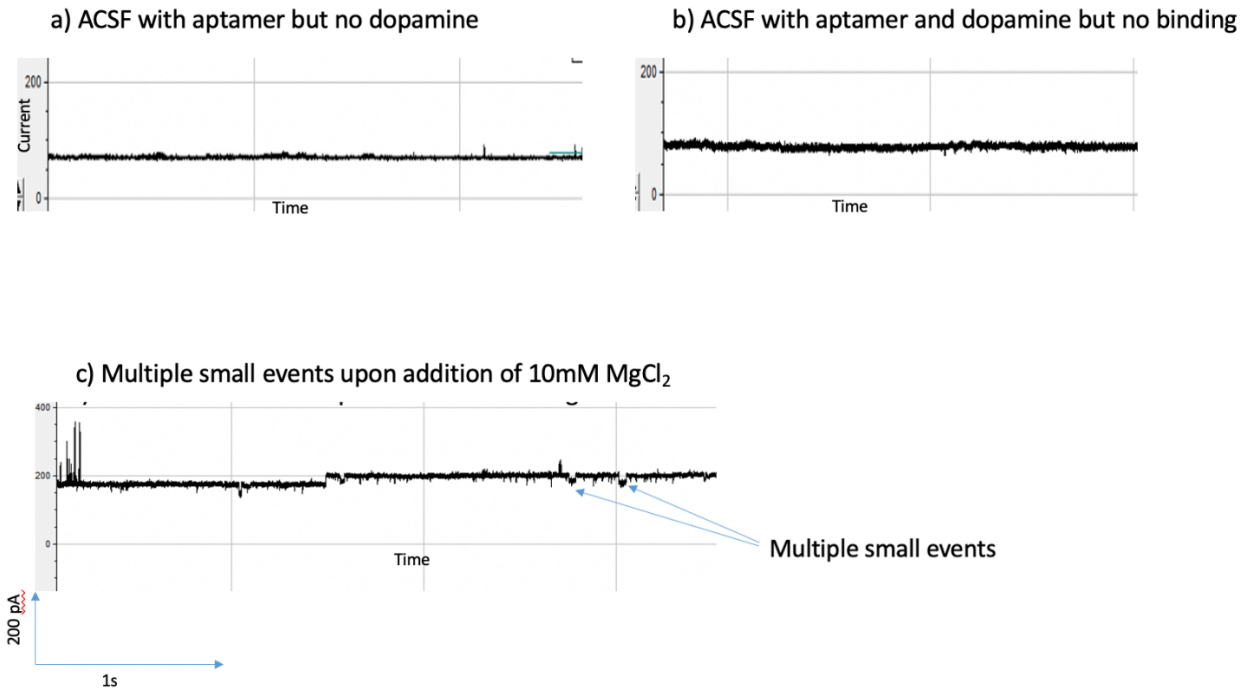

Fig 4. 7: Measuring dopamine at physiological concentration.

a) When the aptamer was added to the cis side no events were observed. b) There were no events and no evidence of dopamine binding in ACSF. c) Multiple small events were observed when 10mM MgCl2 was added to the cis side.

The next challenge was to determine whether there was evidence of dopamine binding in these events. To achieve this, histograms of the blocked current amplitudes were generated for every detected event. A clear pattern imaged. There were two types of histograms. The first had only one peak as depicted by a representative trace in Fig 4.11 below. This set of histograms could be described by a neatly fitting gaussian distribution. This was interpreted to mean that the amplitudes captured by the histogram were from a single conformational state. These histograms were to histograms generated from the experiments conducted on the aptamer only in the absence of dopamine. There was good concordance between these two sets of histograms in terms of shape, mean current and standard deviation (161.3 pA and std=0.26) and (161.4 and

std=0.29). The second type of histogram had two peaks. The mean blocked current was 160.1 with a standard deviation of 0.74. The standard deviations were statistically significantly different from the deviations obtained from the data without dopamine at the 0.05 level of significance. The two peaks coupled to the statistically significant standard deviations were interpreted to mean that the data captured by these histograms represented two different conformational states. This was indicative of the existence of the two conformational states associated with dopamine binding. Hence it was proved that dopamine was measured in ACSF.

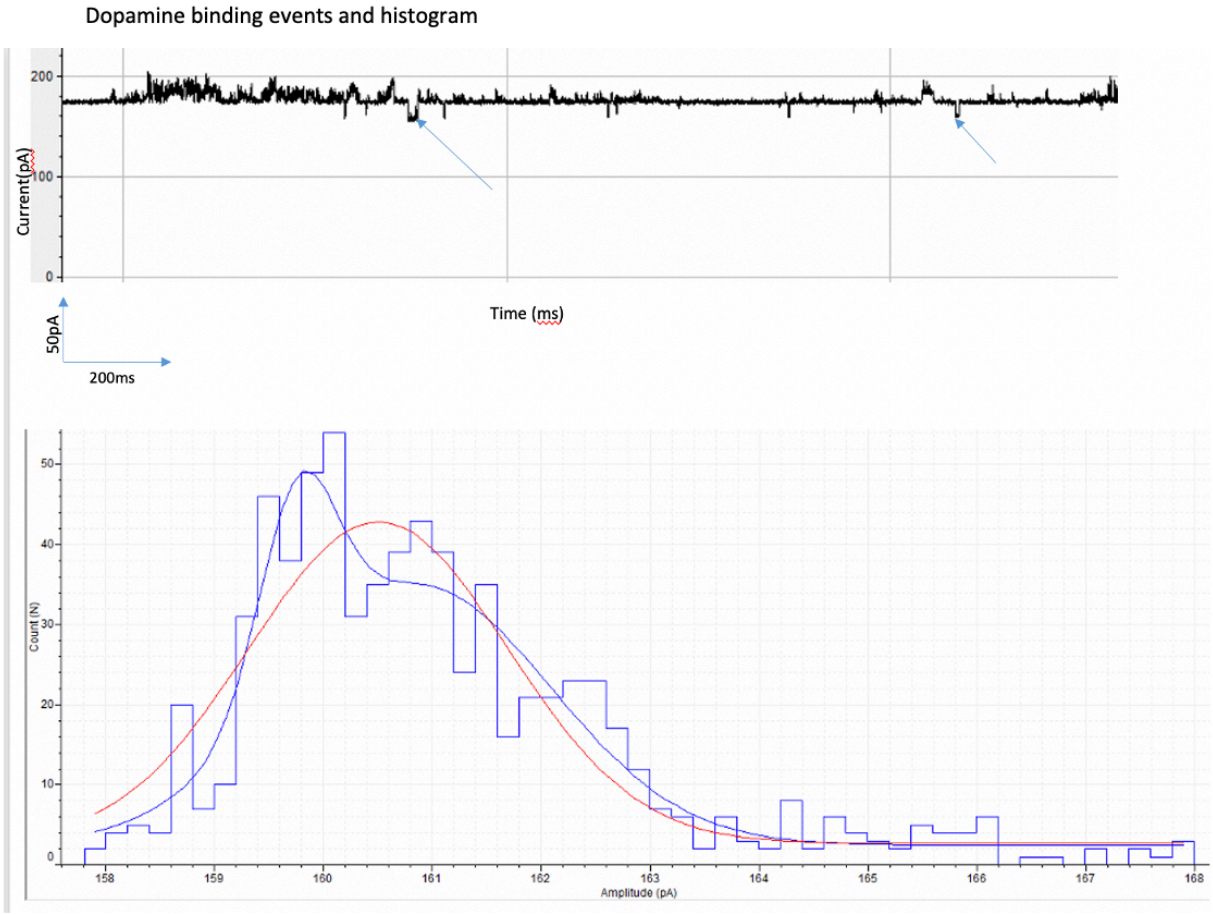

Fig 4. 8: Dopamine binding detected in ACSF.

Events of small magnitude indicating aptamer insertion in pore (see inserted arrows).Histogram of the blocked current amplitudes shows two peaks that fit two overlapping gaussian distributions better than a single gaussian.

4.3.6 Enhancing residence time at high concentrations.

Earlier experiments demonstrated that among the monovalent ions 1M LiCl yielded the longest aptamer residence time. It has also been shown that adding 10mM of $MgCl_2$ increased the residence time obtained using the monovalent ions. To optimize dopamine binding time at higher electrolyte concentrations additional experiments were run with 1M LiCl+10mM $MgCl_2$ using the M7 pore at a bias voltage of 120mV. Residence times of more than 5000ms (median = 4376ms, n=1895) were achieved. This is the combination of experimental conditions that produced the longest binding time and residence time.

4.4 Significance

The biggest challenge with nanopore DNA sequencing is the fast translocation velocities of the DNA. Many labs are focused on efforts to innovate ways of slowing down DNA translocation velocity. Traditionally the experiments are carried out with 1M KCl buffer. Here we have demonstrated an alternative approach. Although our experiments were focused on enhancing dopamine detection we have confirmed earlier reports(Kowalczyk et al., 2012b; Vu et al., 2019; Yan et al., 2019) that monovalent ions with smaller radii, specifically NaCl and LiCl significantly slow down the DNA translocation and produce better read out resolution. Additionally, we have demonstrated that adding 10mM of MgCl2 to the buffer containing monovalent ions significantly increased the residence time of the DNA in the pore. We have also demonstrated for the first time that 200mM MgCl2 on its own produces dwell times that are longer than those produced by 1M KCl buffer. Our findings are therefore extensible to nanopore

sensing and DNA sequencing in general. Divalent ions are an additional tool to aid the efforts to slow down DNA translocation.

4.5 Conclusions

In this chapter we have successfully demonstrated that dopamine detection with the nanopore sensor platform presented in chapter three can be enhanced by tweaking a constellation of factors. Optimization was a multistage process which involved pore selection, bias voltage selection ion type and buffer concentration selection. Furthermore, adding 10mM of MgCl2 further enhanced detection sensitivity. The combination that gave the best result was 1M LiCl at 120mV spiked with 10mM MgCl2. Dopamine detection in physiological concentrations was demonstrated. However, although dopamine detection was achieved in ACSF the read-out resolution was very low. Labor intensity manual histogram generation and curve fitting had to be performed to identify the two-conformation signature indicative of dopamine binding. Improving read-out resolution is a challenge that needs to be addressed. Chapter five will address proposed future directions.

References

Alivisatos, A. P., Chun, M., Church, G. M., Greenspan, R. J., Roukes, M. L., & Yuste, R. (2012).The brain activity map project and the challenge of functional connectomics. *Neuron*, *74*(6), 970–974.

Bai, Y., Greenfeld, M., Travers, K. J., Chu, V. B., Lipfert, J., Doniach, S., & Herschlag, D. (2007). Quantitative and comprehensive decomposition of the ion atmosphere around nucleic acids. *Journal of the American Chemical Society*, *129*(48), 14981–14988.

Bayley, H., & Cremer, P. S. (2001). Stochastic sensors inspired by biology. *Nature*, *413*(6852), 226–230.

Bello, J., Mowla, M., Troise, N., Soyring, J., Borgesi, J., & Shim, J. (2019). Increased dwell time and occurrence of dsDNA translocation events through solid state nanopores by LiCl concentration gradients. *Electrophoresis*, *40*(7), 1082–1090.

Bezrukov, S. M., & Kasianowicz, J. J. (1997). The charge state of an ion channel controls neutral polymer entry into its pore. *European Biophysics Journal*, *26*(6), 471–476.

Bezrukov, S. M., Vodyanoy, I., Brutyan, R. A., & Kasianowicz, J. J. (1996). Dynamics and free energy of polymers partitioning into a nanoscale pore. *Macromolecules*, *29*(26), 8517–8522.

Breiman, L. (2001). Random forests. *Machine Learning*, *45*(1), 5–32.

Butler, T. Z., Pavlenok, M., Derrington, I. M., Niederweis, M., & Gundlach, J. H. (2008). Single-molecule DNA detection with an engineered MspA protein nanopore. *Proceedings of the National Academy of Sciences*, *105*(52), 20647. https://doi.org/10.1073/pnas.0807514106

Cheng, Y., Korolev, N., & Nordenskiöld, L. (2006). Similarities and differences in interaction of K+ and Na+ with condensed ordered DNA. A molecular dynamics computer simulation study. *Nucleic Acids Research*, *34*(2), 686–696.

Cornell, B. A., Braach-Maksvytis, V., King, L., Osman, P., Raguse, B., Wieczorek, L., & Pace, R. (1997). A biosensor that uses ion-channel switches. *Nature*, *387*(6633), 580–583.

Davis, J. C., Furstenthal, L., Desai, A. A., Norris, T., Sutaria, S., Fleming, E., & Ma, P. (2009). The microeconomics of personalized medicine: Today's challenge and tomorrow's promise. *Nature Reviews Drug Discovery*, *8*(4), 279–286. https://doi.org/10.1038/nrd2825

De Marky, N., & Manning, G. S. (1975). On the application of polyelectrolyte limiting laws to the helix–coil transition of DNA. III. Dependence of helix stability on excess univalent salt and on polynucleotide phosphate concentration for variable equivalent ratios of divalent metal ion to phosphate. *Biopolymers: Original Research on Biomolecules*, *14*(7), 1407–1422.

De Marky, N., & Manning, G. S. (1976). On the application of polyelectrolyte limiting laws to the helix–coil transition of DNA. IV. Dependence of helix stability on the concentration of divalent metal ions. *Biopolymers: Original Research on Biomolecules*, *15*(3), 457–468.

de Zoysa, R. S. S., Jayawardhana, D. A., Zhao, Q., Wang, D., Armstrong, D. W., & Guan, X. (2009). Slowing DNA translocation through nanopores using a solution containing organic salts. *The Journal of Physical Chemistry B*, *113*(40), 13332–13336.

Derrington, I. M., Butler, T. Z., Collins, M. D., Manrao, E., Pavlenok, M., Niederweis, M., & Gundlach, J. H. (2010). Nanopore DNA sequencing with MspA. *Proceedings of the National Academy of Sciences*, *107*(37), 16060. https://doi.org/10.1073/pnas.1001831107

Dong, Q., Stellwagen, E., & Stellwagen, N. C. (2009). Monovalent cation binding in the minor groove of DNA A-tracts. *Biochemistry*, *48*(5), 1047–1055.

Dove, W. F., & Davidson, N. (1962). Cation effects on the denaturation of DNA. *Journal of Molecular Biology*, *5*(5), 467–478.

Falkenhagen, H. (1931). The principal ideas in the interionic attraction theory of strong electrolytes. *Reviews of Modern Physics*, *3*(3), 412.

Fang, H., Pajski, M. L., Ross, A. E., & Venton, B. J. (2013). Quantitation of dopamine, serotonin and adenosine content in a tissue punch from a brain slice using capillary electrophoresis with fast-scan cyclic voltammetry detection. *Analytical Methods*, *5*(11), 2704–2711.

Fologea, D., Uplinger, J., Thomas, B., McNabb, D. S., & Li, J. (2005). Slowing DNA translocation in a solid-state nanopore. *Nano Letters*, *5*(9), 1734–1737.

Gareth James, D. W., Trevor Hastie, Robert Tibshirani. (2013). *An introduction to statistical learning: With applications in R*. New York : Springer, [2013] ©2013. https://search.library.wisc.edu/catalog/9910207152902121

Grosberg, A. Y., & Rabin, Y. (2010). DNA capture into a nanopore: Interplay of diffusion and electrohydrodynamics. *The Journal of Chemical Physics*, *133*(16), 10B617.

Guéroult, M., Boittin, O., Mauffret, O., Etchebest, C., & Hartmann, B. (2012). Mg 2+ in the major groove modulates B-DNA structure and dynamics. *PloS One*, *7*(7), e41704.

H. B. Mann & D. R. Whitney. (1947). On a Test of Whether one of Two Random Variables is Stochastically Larger than the Other. *The Annals of Mathematical Statistics*, *18*(1), 50–60. https://doi.org/10.1214/aoms/1177730491

He, Y., Tsutsui, M., Scheicher, R. H., Fan, C., Taniguchi, M., & Kawai, T. (2013). Mechanism of how salt-gradient-induced charges affect the translocation of DNA molecules through a nanopore. *Biophysical Journal*, *105*(3), 776–782.

Heddi, B., Foloppe, N., Hantz, E., & Hartmann, B. (2007). The DNA structure responds differently to physiological concentrations of K+ or Na+. *Journal of Molecular Biology*, *368*(5), 1403–1411.

Heng, J. B., Ho, C., Kim, T., Timp, R., Aksimentiev, A., Grinkova, Y. V., Sligar, S., Schulten, K., & Timp, G. (2004). Sizing DNA using a nanometer-diameter pore. *Biophysical Journal*, *87*(4), 2905–2911.

Henrickson, S. E., Misakian, M., Robertson, B., & Kasianowicz, J. J. (2000). Driven DNA transport into an asymmetric nanometer-scale pore. *Physical Review Letters*, *85*(14), 3057.

Hud, N. V., & Plavec, J. (2003). A unified model for the origin of DNA sequence-directed curvature. *Biopolymers: Original Research on Biomolecules*, *69*(1), 144–158.

Hyman, S. E. (2005). Neurotransmitters. *Current Biology*, *15*(5), R154–R158.

Kasianowicz, J. J., Brandin, E., Branton, D., & Deamer, D. W. (1996). Characterization of individual polynucleotide molecules using a membrane channel. *Proceedings of the National Academy of Sciences*, *93*(24), 13770–13773.

Korolev, N., Lyubartsev, A. P., Rupprecht, A., & Nordenskiöld, L. (1999). Competitive binding of Mg2+, Ca2+, Na+, and K+ ions to DNA in oriented DNA fibers: Experimental and Monte Carlo simulation results. *Biophysical Journal*, *77*(5), 2736–2749.

Kowalczyk, S. W., Wells, D. B., Aksimentiev, A., & Dekker, C. (2012a). Slowing down DNA translocation through a nanopore in lithium chloride. *Nano Letters*, *12*(2), 1038–1044.

Kowalczyk, S. W., Wells, D. B., Aksimentiev, A., & Dekker, C. (2012b). Slowing down DNA translocation through a nanopore in lithium chloride. *Nano Letters*, *12*(2), 1038–1044.

Laszlo, A. H., Derrington, I. M., & Gundlach, J. H. (2016). MspA nanopore as a single-molecule tool: From sequencing to SPRNT. *Methods*, *105*, 75–89.

Ledolter, J., & Kardon, R. H. (2020). Focus on data: Statistical design of experiments and sample size selection using power analysis. *Investigative Ophthalmology & Visual Science*, *61*(8), 11–11.

Li, X., Wang, L., & Sung, E. (2008). AdaBoost with SVM-based component classifiers. *Engineering Applications of Artificial Intelligence*, *21*(5), 785–795.

Loman, N. J., Quick, J., & Simpson, J. T. (2015). A complete bacterial genome assembled de novo using only nanopore sequencing data. *Nature Methods*, *12*(8), 733–735.

Lubensky, D. K., & Nelson, D. R. (1999). Driven polymer translocation through a narrow pore. *Biophysical Journal*, *77*(4), 1824–1838.

Maglia, G., Restrepo, M. R., Mikhailova, E., & Bayley, H. (2008). Enhanced translocation of single DNA molecules through α-hemolysin nanopores by manipulation

of internal charge. *Proceedings of the National Academy of Sciences*, *105*(50), 19720–19725.

Manning, G. S. (1978). The molecular theory of polyelectrolyte solutions with applications to the electrostatic properties of polynucleotides. *Quarterly Reviews of Biophysics*, *11*(2), 179–246.

Manrao EA, Derrington IM, Pavlenok M, Niederweis M, Gundlach JH. (2011). Nucleotide Discrimination with DNA Immobilized in the MspA Nanopore. *PLoS ONE 6*, *6*(10).

Marcus, Y. (1997). Ion Properties, Marcus Dekker. *Inc, New York*.

Martin, H. S., Jha, S., Howorka, S., & Coveney, P. V. (2009). Determination of free energy profiles for the translocation of polynucleotides through α-hemolysin nanopores using non-equilibrium molecular dynamics simulations. *Journal of Chemical Theory and Computation*, *5*(8), 2135–2148.

McConnell, K. J., & Beveridge, D. (2000). DNA structure: What's in charge? *Journal of Molecular Biology*, *304*(5), 803–820.

McFail-Isom, L., Sines, C. C., & Williams, L. D. (1999). DNA structure: Cations in charge? *Current Opinion in Structural Biology*, *9*(3), 298–304.

Meller, A. (2003). Dynamics of polynucleotide transport through nanometre-scale pores. *Journal of Physics: Condensed Matter*, *15*(17), R581.

Meller, A., Nivon, L., Brandin, E., Golovchenko, J., & Branton, D. (2000). Rapid nanopore discrimination between single polynucleotide molecules. *Proceedings of the National Academy of Sciences*, *97*(3), 1079. https://doi.org/10.1073/pnas.97.3.1079

Meller, Amit and Nivon, Lucas and Branton, Daniel. (2001). Voltage-Driven DNA Translocations through a Nanopore. *Phys. Rev. Lett*, *86*(15), 3435–3438.

Movileanu, L., Schmittschmitt, J. P., Scholtz, J. M., & Bayley, H. (2005). Interactions of peptides with a protein pore. *Biophysical Journal*, *89*(2), 1030–1045.

Narahashi, T. (2000). Neuroreceptors and ion channels as the basis for drug action: Past, present, and future. *Journal of Pharmacology and Experimental Therapeutics*, *294*(1), 1–26.

Ou, Y., Buchanan, A. M., Witt, C. E., & Hashemi, P. (2019). Frontiers in electrochemical sensors for neurotransmitter detection: Towards measuring neurotransmitters as chemical diagnostics for brain disorders. *Analytical Methods*, *11*(21), 2738–2755.

Owczarzy, R., Moreira, B. G., You, Y., Behlke, M. A., & Walder, J. A. (2008). Predicting stability of DNA duplexes in solutions containing magnesium and monovalent cations. *Biochemistry*, *47*(19), 5336–5353.

Schreiber, J., & Karplus, K. (2015). Analysis of nanopore data using hidden Markov models. *Bioinformatics*, *31*(12), 1897–1903.

Simpson, J. T., Workman, R. E., Zuzarte, P., David, M., Dursi, L., & Timp, W. (2017). Detecting DNA cytosine methylation using nanopore sequencing. *Nature Methods*, *14*(4), 407–410.

Smeets, R. M., Keyser, U. F., Krapf, D., Wu, M.-Y., Dekker, N. H., & Dekker, C. (2006). Salt dependence of ion transport and DNA translocation through solid-state nanopores. *Nano Letters*, *6*(1), 89–95.

Stellwagen, E., Dong, Q., & Stellwagen, N. C. (2005). Monovalent cations affect the free solution mobility of DNA by perturbing the hydrogen-bonded structure of water. *Biopolymers: Original Research on Biomolecules*, *78*(2), 62–68.

Stellwagen, N. C., Gelfi, C., & Righetti, P. G. (1997). The free solution mobility of DNA. *Biopolymers: Original Research on Biomolecules*, *42*(6), 687–703.

Storm, A. J., Storm, C., Chen, J., Zandbergen, H., Joanny, J.-F., & Dekker, C. (2005). Fast DNA translocation through a solid-state nanopore. *Nano Letters*, *5*(7), 1193–1197.

Subirana, J. A., & Soler-Lopez, M. (2003). Cations as hydrogen bond donors: A view of electrostatic interactions in DNA. *Annual Review of Biophysics and Biomolecular Structure*, *32*(1), 27–45.

Sung, W., & Park, P. (1996). Polymer translocation through a pore in a membrane. *Physical Review Letters*, *77*(4), 783.

Thomas J. DiCiccio & Bradley Efron. (1996). Bootstrap confidence intervals. *Statistical Science*, *11*(3), 189–228. https://doi.org/10.1214/ss/1032280214

Timp, W., Comer, J., & Aksimentiev, A. (2012). DNA base-calling from a nanopore using a Viterbi algorithm. *Biophysical Journal*, *102*(10), L37–L39.

Van den Hout, M., Krudde, V., Janssen, X. J., & Dekker, N. H. (2010). Distinguishable populations report on the interactions of single DNA molecules with solid-state nanopores. *Biophysical Journal*, *99*(11), 3840–3848.

Van Dorp, S., Keyser, U. F., Dekker, N. H., Dekker, C., & Lemay, S. G. (2009). Origin of the electrophoretic force on DNA in solid-state nanopores. *Nature Physics*, *5*(5), 347–351.

Vu, T., Borgesi, J., Soyring, J., D'Alia, M., Davidson, S.-L., & Shim, J. (2019). Employing LiCl salt gradient in the wild-type α-hemolysin nanopore to slow down DNA translocation and detect methylated cytosine. *Nanoscale*, *11*(21), 10536–10545.

Wang, L., & Fu, X. (2006). *Data mining with computational intelligence*. Springer Science & Business Media.

Wanunu, M., Morrison, W., Rabin, Y., Grosberg, A. Y., & Meller, A. (2010a). Electrostatic focusing of unlabelled DNA into nanoscale pores using a salt gradient. *Nature Nanotechnology*, *5*(2), 160–165.

Wanunu, M., Morrison, W., Rabin, Y., Grosberg, A. Y., & Meller, A. (2010b). Electrostatic focusing of unlabelled DNA into nanoscale pores using a salt gradient. *Nature Nanotechnology*, *5*(2), 160–165.

Wanunu, M., Sutin, J., McNally, B., Chow, A., & Meller, A. (2008). DNA translocation governed by interactions with solid-state nanopores. *Biophysical Journal*, *95*(10), 4716–4725.

Yan, H., Zhou, D., Shi, B., Zhang, Z., Tian, H., Yu, L., Wang, Y., Guan, X., Wang, Z., & Wang, D. (2019). Slowing down DNA translocation velocity using a LiCl salt gradient and nanofiber mesh. *European Biophysics Journal*, *48*(3), 261–266.

Yeh, I.-C., & Hummer, G. (2004). Nucleic acid transport through carbon nanotube membranes. *Proceedings of the National Academy of Sciences*, *101*(33), 12177–12182.

Yeh, L., Zhang, M., Joo, S. W., & Qian, S. (2012). Slowing down DNA translocation through a nanopore by lowering fluid temperature. *Electrophoresis*, *33*(23), 3458–3465.

Yoo, J., & Aksimentiev, A. (2012). Competitive binding of cations to duplex DNA revealed through molecular dynamics simulations. *The Journal of Physical Chemistry B*, *116*(43), 12946–12954.

Zhang, H., Zhao, Q., Tang, Z., Liu, S., Li, Q., Fan, Z., Yang, F., You, L., Li, X., & Zhang, J. (2013). Slowing down DNA translocation through solid-state nanopores by pressure. *Small*, *9*(24), 4112–4117.

Chapter Five

Future Directions

5.1 Introduction

The overarching goal of this project was to develop a platform for label-free detection of small molecule-induced single nucleic acid molecule time-resolved conformational transitions in an aptamer-inlaid nanopore. Time resolved conformational changes were demonstrated at different concentrations using different ion types. Additionally, the unique combination of experimental conditions that produce the best read-out resolution and sensitivity was established. Poor resolution in lower concentration remains problematic. This chapter proposes future directions aimed at addressing this problem among others.

5.2.1 Further mutant exploration

The current project focused on two mutants of the MspA pore. The structure of the pore is depicted in Fig 5.1 below. These mutants M2 and M7 were created by altering the charge distribution of the R118 and R134 rings of residues, which are in the vestibule and the entrance region respectively. The distribution of charges in the constriction of the pore were not altered. Previously it was reported that when the rings of residues in the constriction zone (shown as D90, D91 and D93) in Fig 5.1 as in the wild type the pore did not allow DNA translocation(Derrington et al., 2010). The importance of DNA-pore interactions was previously articulated(Bezrukov et al., 1996; Bezrukov & Kasianowicz, 1997; Lubensky & Nelson, 1999). The interactions were of greater magnitude in narrow pores. In the case of the MspA pore the

constriction is 1nm wide. Hence the interactions between the DNA and the charges in this zone will be expected to be greater in magnitude than those in the pore entrance and the vestibule. In previous work the charge distribution in the pore was neutral ostensibly to facilitate the translocation of the negatively charged DNA. However, the goal of this work is better achieved by anchoring the DNA in the pore for a longer duration. What is the impact of replacing some of the neutral rings with positively charged residues? Will, for example changing D90 and D91 to positive rings create another zone in which DNA is anchored? In the current study we concluded that the R118 ring is the location where the DNA is captured. Intuitively it would seem that creating more capture zones would produce at two desirable outcomes. Firstly, it will slow down the DNA even more. Secondly, it might create a stepwise translocation pattern in which the DNA is briefly captured in one site before moving and getting trapped in another site before eventually translocating. In principle this slow down the DNA and yield traces with better readout resolution.

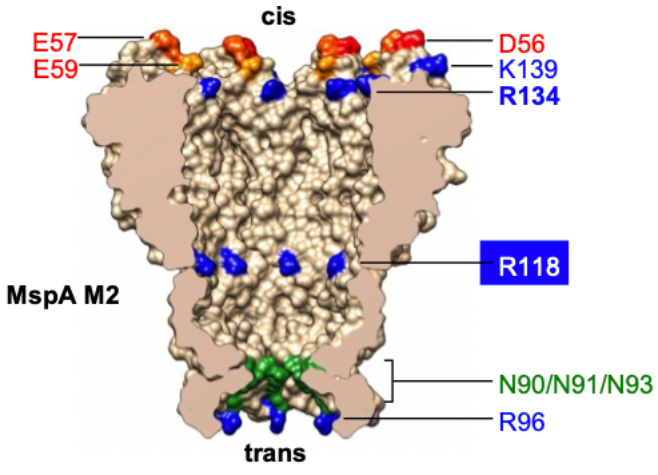

Fig 5.1 The MspA pore structure.

There is also a need to increase the sensitivity to neurotransmitters to the nM range. Moreover, the aptamer can also be engineered to shorten the binding time of the neurotransmitter to increase the number of binding events per aptamer. Finally, the aptamer-inlaid nanopore can be integrated within integrated nanopore systems (e.g., Oxford Nanopore) for high-throughput neurochemistry or used in nanopore-terminated probes to achieve both high spatial- and temporal-resolution. In a nutshell, there is scope to explore the impact of different mutations.

5.2.2 Improving stability of lipid bilayer

Previously it was reported that DNA translocation velocity could be significantly slowed done by employing salt gradients(Bello et al., 2019; He et al., 2013; Vu et al., 2019; Wanunu et al., 2010a; Yan et al., 2019). Additionally, it is the finding of the current study that dopamine binding increased with increasing salt concentration. (Wanunu et al., 2010a) reported that by applying a 20-fold salt gradient across the pore, nanopore sensitivity was improved by a factor of 40. Most of the experiments employing salt gradients in the literature used synthetic nanopores(Bello et al., 2019; Wanunu et al., 2010a; Yan et al., 2019). (Vu et al., 2019) achieved a 6-fold increase in DNA capture rate by employing a 15-fold salt gradient of LiCl with an alpha hemolysin pore. However, attempts to employ a salt gradient experimental design at higher salt concentrations was hampered by unstable bilayers. Bilayer stability is critical in nanopore sensing. New techniques should be developed to improve the stability of the bilayer. Approaches could include tethering the lipid bilayer on solid supports(Cornell et al., 1997).

5.2.3 Machine learning and artificial intelligence approach to data analysis

Broadly the approach to dopamine detection and measurement adopted involved two steps. In the first step a reference signature pattern was established. The second step involved comparing the signature generated in an experiment to the reference. Successful detection was determined by a concordance between the reference pattern and the experimental pattern. This

process was performed manually. Not only is it cumbersome, but it also slows down the throughput. Rapid throughput requires a different approach.

Automated approaches to dopamine detection and measurement can replace manual processing. Several authors have demonstrated that hidden Markov models(HMMs) can be used to analyze nanopore data(Loman et al., 2015; Schreiber & Karplus, 2015; Simpson et al., 2017; Timp et al., 2012). Furthermore, classic classifiers such as Bayesian classifier, random forest

and support vector machine have already been widely and successfully deployed in bioinformatics(Breiman, 2001; Li et al., 2008; Wang & Fu, 2006, 2006). The same methods can be extended to neurotransmitter detection using nanopore sensing. In essence the output from a nanopore sensing experiment is an electrical signal that lends itself to prosaic electrical signal processing approaches. This should make the process of identifying features to use as the basis for pattern recognition achievable. The focus should be on identifying the minimum set of features required for identification of dopamine detection. The significance of establishing the minimum features lies in that it reduces the computational burden and reduces the turnaround time.

The next step after the development of algorithms and models would be to train them and then apply them to data samples containing pre-identified dopamine binding events. This would be used as the foundation for developing receiver operating curves and data classification protocols.

5.2.4 Molecular Dynamics simulations to elucidate the microscopic mechanism of residence time dependence on ion type and concentration.

One significant finding of the current study was the pronounced impact of the addition of 10mM MgCl2 to the electrolyte on the aptamer residence time. MgCl2 was not only necessary for dopamine detection in low concentration, but on its own it was sufficient at 200mM to

demonstrate dopamine binding. Many explanations were suggested including the increased affinity of DNA for smaller ions and the increased charge screening provided by divalent ions. All atom molecular dynamics (MD) simulations can deepen our understanding of the processes and forces at play.

Broadly, the MD simulations can have the following aims:

(i) To simulate the dependence of the stall force on the type and concentration of the ion at different nanopore diameters.

(ii) To extend the simulations to DNA molecules of different lengths.

The deliverable from the simulations should be an elaborate characterization of the effective charge of the DNA in monovalent and divalent electrolytes of various concentrations and in multi-electrolyte solutions.

References

Alivisatos, A. P., Chun, M., Church, G. M., Greenspan, R. J., Roukes, M. L., & Yuste, R. (2012). The brain activity map project and the challenge of functional connectomics. *Neuron*, *74*(6), 970–974.

Bai, Y., Greenfeld, M., Travers, K. J., Chu, V. B., Lipfert, J., Doniach, S., & Herschlag, D. (2007). Quantitative and comprehensive decomposition of the ion atmosphere around nucleic acids. *Journal of the American Chemical Society*, *129*(48), 14981–14988.

Bayley, H., & Cremer, P. S. (2001). Stochastic sensors inspired by biology. *Nature*, *413*(6852), 226–230.

Bello, J., Mowla, M., Troise, N., Soyring, J., Borgesi, J., & Shim, J. (2019). Increased dwell time and occurrence of dsDNA translocation events through solid state nanopores by LiCl concentration gradients. *Electrophoresis*, *40*(7), 1082–1090.

Bezrukov, S. M., & Kasianowicz, J. J. (1997). The charge state of an ion channel controls neutral polymer entry into its pore. *European Biophysics Journal*, *26*(6), 471–476.

Bezrukov, S. M., Vodyanoy, I., Brutyan, R. A., & Kasianowicz, J. J. (1996). Dynamics and free energy of polymers partitioning into a nanoscale pore. *Macromolecules*, *29*(26), 8517–8522.

Breiman, L. (2001). Random forests. *Machine Learning*, *45*(1), 5–32.

Butler, T. Z., Pavlenok, M., Derrington, I. M., Niederweis, M., & Gundlach, J. H. (2008). Single-molecule DNA detection with an engineered MspA protein nanopore. *Proceedings of the National Academy of Sciences*, *105*(52), 20647. https://doi.org/10.1073/pnas.0807514106

Cheng, Y., Korolev, N., & Nordenskiöld, L. (2006). Similarities and differences in interaction of K+ and Na+ with condensed ordered DNA. A molecular dynamics computer simulation study. *Nucleic Acids Research*, *34*(2), 686–696.

Cornell, B. A., Braach-Maksvytis, V., King, L., Osman, P., Raguse, B., Wieczorek, L., & Pace, R. (1997). A biosensor that uses ion-channel switches. *Nature*, *387*(6633), 580–583.

Davis, J. C., Furstenthal, L., Desai, A. A., Norris, T., Sutaria, S., Fleming, E., & Ma, P. (2009). The microeconomics of personalized medicine: Today's challenge and tomorrow's promise. *Nature Reviews Drug Discovery*, *8*(4), 279–286. https://doi.org/10.1038/nrd2825

De Marky, N., & Manning, G. S. (1975). On the application of polyelectrolyte limiting laws to the helix–coil transition of DNA. III. Dependence of helix stability on excess univalent salt and on polynucleotide phosphate concentration for variable equivalent ratios of divalent metal ion to phosphate. *Biopolymers: Original Research on Biomolecules*, *14*(7), 1407–1422.

De Marky, N., & Manning, G. S. (1976). On the application of polyelectrolyte limiting laws to the helix–coil transition of DNA. IV. Dependence of helix stability on the concentration of divalent metal ions. *Biopolymers: Original Research on Biomolecules*, *15*(3), 457–468.

de Zoysa, R. S. S., Jayawardhana, D. A., Zhao, Q., Wang, D., Armstrong, D. W., & Guan, X. (2009). Slowing DNA translocation through nanopores using a solution containing organic salts. *The Journal of Physical Chemistry B*, *113*(40), 13332–13336.

Derrington, I. M., Butler, T. Z., Collins, M. D., Manrao, E., Pavlenok, M., Niederweis, M., & Gundlach, J. H. (2010). Nanopore DNA sequencing with MspA. *Proceedings of the National Academy of Sciences*, *107*(37), 16060. https://doi.org/10.1073/pnas.1001831107

Dong, Q., Stellwagen, E., & Stellwagen, N. C. (2009). Monovalent cation binding in the minor groove of DNA A-tracts. *Biochemistry*, *48*(5), 1047–1055.

Dove, W. F., & Davidson, N. (1962). Cation effects on the denaturation of DNA. *Journal of Molecular Biology*, *5*(5), 467–478.

Falkenhagen, H. (1931). The principal ideas in the interionic attraction theory of strong electrolytes. *Reviews of Modern Physics*, *3*(3), 412.

Fang, H., Pajski, M. L., Ross, A. E., & Venton, B. J. (2013). Quantitation of dopamine, serotonin and adenosine content in a tissue punch from a brain slice using capillary electrophoresis with fast-scan cyclic voltammetry detection. *Analytical Methods*, *5*(11), 2704–2711.

Fologea, D., Uplinger, J., Thomas, B., McNabb, D. S., & Li, J. (2005). Slowing DNA translocation in a solid-state nanopore. *Nano Letters*, *5*(9), 1734–1737.

Gareth James, D. W., Trevor Hastie, Robert Tibshirani. (2013). *An introduction to statistical learning: With applications in R*. New York : Springer, [2013] ©2013. https://search.library.wisc.edu/catalog/9910207152902121

Grosberg, A. Y., & Rabin, Y. (2010). DNA capture into a nanopore: Interplay of diffusion and electrohydrodynamics. *The Journal of Chemical Physics*, *133*(16), 10B617.

Guéroult, M., Boittin, O., Mauffret, O., Etchebest, C., & Hartmann, B. (2012). Mg 2+ in the major groove modulates B-DNA structure and dynamics. *PloS One*, *7*(7), e41704.

H. B. Mann & D. R. Whitney. (1947). On a Test of Whether one of Two Random Variables is Stochastically Larger than the Other. *The Annals of Mathematical Statistics*, *18*(1), 50–60. https://doi.org/10.1214/aoms/1177730491

He, Y., Tsutsui, M., Scheicher, R. H., Fan, C., Taniguchi, M., & Kawai, T. (2013). Mechanism of how salt-gradient-induced charges affect the translocation of DNA molecules through a nanopore. *Biophysical Journal*, *105*(3), 776–782.

Heddi, B., Foloppe, N., Hantz, E., & Hartmann, B. (2007). The DNA structure responds differently to physiological concentrations of K+ or Na+. *Journal of Molecular Biology*, *368*(5), 1403–1411.

Heng, J. B., Ho, C., Kim, T., Timp, R., Aksimentiev, A., Grinkova, Y. V., Sligar, S., Schulten, K., & Timp, G. (2004). Sizing DNA using a nanometer-diameter pore. *Biophysical Journal*, *87*(4), 2905–2911.

Henrickson, S. E., Misakian, M., Robertson, B., & Kasianowicz, J. J. (2000). Driven DNA transport into an asymmetric nanometer-scale pore. *Physical Review Letters*, *85*(14), 3057.

Hud, N. V., & Plavec, J. (2003). A unified model for the origin of DNA sequence-directed curvature. *Biopolymers: Original Research on Biomolecules*, *69*(1), 144–158.

Hyman, S. E. (2005). Neurotransmitters. *Current Biology*, *15*(5), R154–R158.

Kasianowicz, J. J., Brandin, E., Branton, D., & Deamer, D. W. (1996). Characterization of individual polynucleotide molecules using a membrane channel. *Proceedings of the National Academy of Sciences*, *93*(24), 13770–13773.

Korolev, N., Lyubartsev, A. P., Rupprecht, A., & Nordenskiöld, L. (1999). Competitive binding of Mg2+, Ca2+, Na+, and K+ ions to DNA in oriented DNA fibers: Experimental and Monte Carlo simulation results. *Biophysical Journal*, *77*(5), 2736–2749.

Kowalczyk, S. W., Wells, D. B., Aksimentiev, A., & Dekker, C. (2012a). Slowing down DNA translocation through a nanopore in lithium chloride. *Nano Letters*, *12*(2), 1038–1044.

Kowalczyk, S. W., Wells, D. B., Aksimentiev, A., & Dekker, C. (2012b). Slowing down DNA translocation through a nanopore in lithium chloride. *Nano Letters*, *12*(2), 1038–1044.

Laszlo, A. H., Derrington, I. M., & Gundlach, J. H. (2016). MspA nanopore as a single-molecule tool: From sequencing to SPRNT. *Methods*, *105*, 75–89.

Ledolter, J., & Kardon, R. H. (2020). Focus on data: Statistical design of experiments and sample size selection using power analysis. *Investigative Ophthalmology & Visual Science*, *61*(8), 11–11.

Li, X., Wang, L., & Sung, E. (2008). AdaBoost with SVM-based component classifiers. *Engineering Applications of Artificial Intelligence*, *21*(5), 785–795.

Loman, N. J., Quick, J., & Simpson, J. T. (2015). A complete bacterial genome assembled de novo using only nanopore sequencing data. *Nature Methods*, *12*(8), 733–735.

Lubensky, D. K., & Nelson, D. R. (1999). Driven polymer translocation through a narrow pore. *Biophysical Journal*, *77*(4), 1824–1838.

Maglia, G., Restrepo, M. R., Mikhailova, E., & Bayley, H. (2008). Enhanced translocation of single DNA molecules through α-hemolysin nanopores by manipulation

of internal charge. *Proceedings of the National Academy of Sciences*, *105*(50), 19720–19725.

Manning, G. S. (1978). The molecular theory of polyelectrolyte solutions with applications to the electrostatic properties of polynucleotides. *Quarterly Reviews of Biophysics*, *11*(2), 179–246.

Manrao EA, Derrington IM, Pavlenok M, Niederweis M, Gundlach JH. (2011). Nucleotide Discrimination with DNA Immobilized in the MspA Nanopore. *PLoS ONE 6*, *6*(10).

Marcus, Y. (1997). Ion Properties, Marcus Dekker. *Inc, New York*.

Martin, H. S., Jha, S., Howorka, S., & Coveney, P. V. (2009). Determination of free energy profiles for the translocation of polynucleotides through α-hemolysin nanopores using non-equilibrium molecular dynamics simulations. *Journal of Chemical Theory and Computation*, *5*(8), 2135–2148.

McConnell, K. J., & Beveridge, D. (2000). DNA structure: What's in charge? *Journal of Molecular Biology*, *304*(5), 803–820.

McFail-Isom, L., Sines, C. C., & Williams, L. D. (1999). DNA structure: Cations in charge? *Current Opinion in Structural Biology*, *9*(3), 298–304.

Meller, A. (2003). Dynamics of polynucleotide transport through nanometre-scale pores. *Journal of Physics: Condensed Matter*, *15*(17), R581.

Meller, A., Nivon, L., Brandin, E., Golovchenko, J., & Branton, D. (2000). Rapid nanopore discrimination between single polynucleotide molecules. *Proceedings of the National Academy of Sciences*, *97*(3), 1079. https://doi.org/10.1073/pnas.97.3.1079

Meller, Amit and Nivon, Lucas and Branton, Daniel. (2001). Voltage-Driven DNA Translocations through a Nanopore. *Phys. Rev. Lett*, *86*(15), 3435–3438.

Movileanu, L., Schmittschmitt, J. P., Scholtz, J. M., & Bayley, H. (2005). Interactions of peptides with a protein pore. *Biophysical Journal*, *89*(2), 1030–1045.

Narahashi, T. (2000). Neuroreceptors and ion channels as the basis for drug action: Past, present, and future. *Journal of Pharmacology and Experimental Therapeutics*, *294*(1), 1–26.

Ou, Y., Buchanan, A. M., Witt, C. E., & Hashemi, P. (2019). Frontiers in electrochemical sensors for neurotransmitter detection: Towards measuring neurotransmitters as chemical diagnostics for brain disorders. *Analytical Methods*, *11*(21), 2738–2755.

Owczarzy, R., Moreira, B. G., You, Y., Behlke, M. A., & Walder, J. A. (2008). Predicting stability of DNA duplexes in solutions containing magnesium and monovalent cations. *Biochemistry*, *47*(19), 5336–5353.

Schreiber, J., & Karplus, K. (2015). Analysis of nanopore data using hidden Markov models. *Bioinformatics*, *31*(12), 1897–1903.

Simpson, J. T., Workman, R. E., Zuzarte, P., David, M., Dursi, L., & Timp, W. (2017). Detecting DNA cytosine methylation using nanopore sequencing. *Nature Methods*, *14*(4), 407–410.

Smeets, R. M., Keyser, U. F., Krapf, D., Wu, M.-Y., Dekker, N. H., & Dekker, C. (2006). Salt dependence of ion transport and DNA translocation through solid-state nanopores. *Nano Letters*, *6*(1), 89–95.

Stellwagen, E., Dong, Q., & Stellwagen, N. C. (2005). Monovalent cations affect the free solution mobility of DNA by perturbing the hydrogen-bonded structure of water. *Biopolymers: Original Research on Biomolecules*, *78*(2), 62–68.

Stellwagen, N. C., Gelfi, C., & Righetti, P. G. (1997). The free solution mobility of DNA. *Biopolymers: Original Research on Biomolecules*, *42*(6), 687–703.

Storm, A. J., Storm, C., Chen, J., Zandbergen, H., Joanny, J.-F., & Dekker, C. (2005). Fast DNA translocation through a solid-state nanopore. *Nano Letters*, *5*(7), 1193–1197.

Subirana, J. A., & Soler-Lopez, M. (2003). Cations as hydrogen bond donors: A view of electrostatic interactions in DNA. *Annual Review of Biophysics and Biomolecular Structure*, *32*(1), 27–45.

Sung, W., & Park, P. (1996). Polymer translocation through a pore in a membrane. *Physical Review Letters*, *77*(4), 783.

Thomas J. DiCiccio & Bradley Efron. (1996). Bootstrap confidence intervals. *Statistical Science*, *11*(3), 189–228. https://doi.org/10.1214/ss/1032280214

Timp, W., Comer, J., & Aksimentiev, A. (2012). DNA base-calling from a nanopore using a Viterbi algorithm. *Biophysical Journal*, *102*(10), L37–L39.

Van den Hout, M., Krudde, V., Janssen, X. J., & Dekker, N. H. (2010). Distinguishable populations report on the interactions of single DNA molecules with solid-state nanopores. *Biophysical Journal*, *99*(11), 3840–3848.

Van Dorp, S., Keyser, U. F., Dekker, N. H., Dekker, C., & Lemay, S. G. (2009). Origin of the electrophoretic force on DNA in solid-state nanopores. *Nature Physics*, *5*(5), 347–351.

Vu, T., Borgesi, J., Soyring, J., D'Alia, M., Davidson, S.-L., & Shim, J. (2019). Employing LiCl salt gradient in the wild-type α-hemolysin nanopore to slow down DNA translocation and detect methylated cytosine. *Nanoscale*, *11*(21), 10536–10545.

Wang, L., & Fu, X. (2006). *Data mining with computational intelligence*. Springer Science & Business Media.

Wanunu, M., Morrison, W., Rabin, Y., Grosberg, A. Y., & Meller, A. (2010a). Electrostatic focusing of unlabelled DNA into nanoscale pores using a salt gradient. *Nature Nanotechnology*, *5*(2), 160–165.

Wanunu, M., Morrison, W., Rabin, Y., Grosberg, A. Y., & Meller, A. (2010b). Electrostatic focusing of unlabelled DNA into nanoscale pores using a salt gradient. *Nature Nanotechnology*, *5*(2), 160–165.

Wanunu, M., Sutin, J., McNally, B., Chow, A., & Meller, A. (2008). DNA translocation governed by interactions with solid-state nanopores. *Biophysical Journal*, *95*(10), 4716–4725.

Yan, H., Zhou, D., Shi, B., Zhang, Z., Tian, H., Yu, L., Wang, Y., Guan, X., Wang, Z., & Wang, D. (2019). Slowing down DNA translocation velocity using a LiCl salt gradient and nanofiber mesh. *European Biophysics Journal*, *48*(3), 261–266.

Yeh, I.-C., & Hummer, G. (2004). Nucleic acid transport through carbon nanotube membranes. *Proceedings of the National Academy of Sciences*, *101*(33), 12177–12182.

Yeh, L., Zhang, M., Joo, S. W., & Qian, S. (2012). Slowing down DNA translocation through a nanopore by lowering fluid temperature. *Electrophoresis*, *33*(23), 3458–3465.

Yoo, J., & Aksimentiev, A. (2012). Competitive binding of cations to duplex DNA revealed through molecular dynamics simulations. *The Journal of Physical Chemistry B*, *116*(43), 12946–12954.

Zhang, H., Zhao, Q., Tang, Z., Liu, S., Li, Q., Fan, Z., Yang, F., You, L., Li, X., & Zhang, J. (2013). Slowing down DNA translocation through solid-state nanopores by pressure. *Small*, *9*(24), 4112–4117.

VITA

Rugare George Chingarande holds an associate degree in Radiography (Radiation Therapy and Oncology) from the College of Radiographers (London, UK), a bachelors degree in Nuclear Medicine Technology from the University of Johannesburg South Africa and an MBA degree from DeMontfort University (Leicester, UK). Additionally, he holds post graduate diplomas in Health Research Ethics from Stellenbsoch University (South Africa), graduate certificate in Nuclear Engineering (University of Missouri), Graduate minor in Applied Statistics and Graduate Certificate in Neuroscience all from the University of Missouri-Columbia. He worked in several countries in Africa and Europe before pursuing graduate studies at the University of Missouri-Columbia. He will be proceeding to the National Institutes of Health as a visiting post-doctoral fellow.